Title: Variable susceptibility of intestinal organoid-derived monolayers to SARS-CoV-2 infection

Kyung Ku Jang[1], Maria E Kaczmarek[2#], Simone Dallari[1], Ying-Han Chen[1], Takuya Tada[2], Jordan Axelrad[3], Nathaniel R. Landau[2], Kenneth A Stapleford[2*] and Ken Cadwell[1,2,3*]

[1] Kimmel Center for Biology and Medicine at the Skirball Institute, New York University Grossman School of Medicine, New York, NY, USA

[2] Department of Microbiology, New York University Grossman School of Medicine, New York, NY 10016, USA.

[3] Division of Gastroenterology and Hepatology, Department of Medicine, New York University Grossman School of Medicine, New York, NY 10016, USA.

#Present address: EcoHealth Alliance in New York, NY 10018

*Correspondence:
Ken Cadwell
Email: ken.cadwell@med.nyu.edu
Kenneth Stapleford
Email: kenneth.stapleford@nyulangone.org

ABSTRACT

Gastrointestinal effects associated with COVID-19 are highly variable for reasons that are not understood. In this study, we used intestinal organoid-derived cultures differentiated from primary human specimens as a model to examine inter-individual variability. Infection of intestinal organoids derived from different donors with SARS-CoV-2 resulted in orders of magnitude differences in virus replication in small intestinal and colonic organoid-derived monolayers. Susceptibility to infection correlated with *ACE2* expression level and was independent of donor demographic or clinical features. *ACE2* transcript levels in cell culture matched the amount of ACE2 in primary tissue indicating this feature of the intestinal epithelium is retained in the organoids. Longitudinal transcriptomics of organoid-derived monolayers identified a delayed yet robust interferon signature, the magnitude of which corresponded to the degree of SARS-CoV-2 infection. Interestingly, virus with the Omicron variant spike protein infected the organoids with the highest infectivity, suggesting increased tropism of the virus for intestinal tissue. These results suggest that heterogeneity in SARS-CoV-2 replication in intestinal tissues results from differences in ACE2 levels, which may underlie variable patient outcomes.

MAIN TEXT

Intestinal organoid cultures have transformed our ability to investigate properties of the human intestinal epithelium. Consisting of organized epithelial cell clusters differentiated from somatic stem cells, intestinal organoids generated from endoscopic pinch biopsies are capable of self-renewal and recreate many of the structural, functional, and molecular characteristics of the tissue of origin (1). Investigators have exploited these versatile properties of intestinal organoids to study infectious agents that are otherwise difficult to examine, including viruses such as noroviruses (2-4). Intestinal organoids can also inform our understanding of inter-individual differences in disease susceptibility, such as elucidating the mechanisms by which mutations accumulate in patients with colorectal cancer (5, 6). Additionally, we and others have documented substantial heterogeneity in the growth, morphology, viability, and susceptibility to cytokine toxicity of human intestinal organoid lines (1, 6-8). However, how this heterogeneity relates to resistance of the intestinal epithelium to infectious agents remains unclear.

Although severe acute respiratory syndrome coronavirus 2 (SARS-CoV-2) infection is primarily associated with dysfunction of the respiratory system, the gastrointestinal (GI) tract is also an established target organ in patients with COVID-19. As many as 60% of patients present with diarrhea, vomiting, abdominal pain, anorexia, and/or nausea (9-16). Also, SARS-CoV-2 antigen in intestinal biopsies and viral RNA in the stool are readily detected, even after the virus is undetectable in respiratory samples (17-27). To a limited extent, virions and infectious particles have been detected in patient intestinal and stool specimens (17, 25, 28, 29). Although the pathophysiological significance of these observations has not been resolved, the prolonged presence of viral antigens in the gut is likely to impact antibody evolution (17). Consistent with a potential intestinal tropism, intestinal epithelial cells display robust expression of the SARS-CoV-2 receptor angiotensin I converting enzyme 2 (ACE2) and transmembrane proteases TMPRSS2 and TMPRSS4 that facilitate viral entry (30-32). Further, human intestinal organoids derived from either somatic stem cells or inducible pluripotent stem cells (iPSCs) support SARS-CoV-2 reproduction (32-35). These studies have shown that *ACE2* expression levels can differ based on the differentiation state and anatomical region from which the organoids are derived, but whether this affects the degree of SARS-CoV-2 infection is debated. A broader comparison of gene expression patterns and SARS-CoV-2 infection across organoids from different donors and culture conditions may help interpret the studies that have highlighted the extreme range of *ACE2* expression in intestinal tissues associated with demographic and clinical features of individuals, which could have consequences for susceptibility to both viral infections and inflammatory conditions (36-42).

81 Only small numbers of independent small intestinal and colonic organoid lines were
82 compared to one another in previous studies examining SARS-CoV-2 infection of intestinal
83 epithelial cells. Thus, the importance of the anatomical origin of organoids and other variables
84 remains unclear. We established and differentiated 3D organoid lines from small intestinal and
85 colonic biopsies procured from 12 and 13 donors, respectively, from healthy donors and patients
86 with inflammatory bowel disease (IBD) of both sexes (Supplemental Table 1). The expression of
87 *ACE2*, *TMPRSS2,* the enterocyte marker of differentiation *APOA1*, and representative interferon
88 stimulated genes (ISGs) *ISG15*, *OASL*, and *MX2* were significantly higher in small intestinal and
89 colonic organoid lines cultured in 3D differentiation media (3DD) compared with those cultured in
90 expansion media (3DE) that maintains organoids in an undifferentiated state (Supplemental Fig.
91 1A, B, and D-G). *TMPRSS4* expression was similar in both conditions (Supplemental Fig. 1C).
92 Donor-to-donor variability in expression of these genes may reflect the inflammatory environment
93 from which the stem cells were procured. However, 3DE organoids derived from IBD and non-
94 IBD donors displayed comparable gene expression patterns except the decreased *OASL*
95 expression in IBD donor-derived colonic 3DE organoids (Supplemental Fig. 1H). Intestinal
96 organoids can be grown as differentiated monolayers to expose the apical side and facilitate viral
97 entry. We found that the level of *ACE2*, *TMPRSS2*, *TMPRSS4*, *APOA1*, *ISG15*, *OASL*, and *MX2*
98 expression in organoid-derived 2D monolayers correlated well with 3DD organoids generated
99 from the same donor (Fig. 1A-D), suggesting that organoid lines retain their intrinsic gene
100 expression patterns independent of these two culturing conditions. In addition, we found that
101 monolayers exhibited the highest *ACE2* and *TMPRSS2* expression among the culture conditions
102 we examined (Fig. 1E and F) whereas 3DD organoids showed the highest *TMPRSS4*, *APOA1*,
103 *ISG15*, *OASL*, and *MX2* expression (Fig. 1G-K). Therefore, we used the monolayer model to
104 perform all subsequent analyses.
105 We investigated whether *ACE2*, *TMPRSS2*, or *TMPRSS4* expression differed between
106 small intestinal and colonic organoid-derived monolayers. Although *ACE2* expression did not
107 differ, *TMPRSS*2 and *TMPRSS4* expression were higher and *APOA1* was decreased in colonic
108 monolayers (Supplemental Fig. 1I-L). Five pairs of the small intestinal and colonic organoid lines
109 were generated from the same individual. We found that gene expression patterns were generally
110 the same when comparing small intestinal and colonic monolayers from the same donor
111 (Supplemental Fig 2A). The lack of correlation between *ACE2* or *TMPRSS2* expression and
112 *APOA1* expression suggested that heterogeneous *ACE2* and *TMPRSS2* levels were not an
113 artifact caused by insufficient differentiation (Supplemental Fig. 2B and C). When we segregated
114 the data based on disease status or sex, the only difference we observed was decreased *ACE2*

115 and *APOA1* expression in colonic monolayers derived from IBD patients compared with non-IBD
116 donors (Supplemental Fig. 2D-F). The expression of *ISG15*, *OASL,* and *MX2* were also not
117 correlated with disease status or sex (Supplemental Fig. 2E and F), although we note that *ISG15*
118 and *OASL* transcripts were higher in colonic versus small intestinal monolayers (Supplemental
119 Fig. 3A and B). These transcripts generally did not correlate with the age of subjects
120 (Supplemental Table 2).

121 *ACE2* expression differed by as much as 5.9-fold when comparing monolayers with the
122 highest and lowest expression of this gene (Fig. 2A). To test whether such differences lead to
123 heterogeneity in viral infection, we infected monolayers with SARS-CoV-2 at a multiplicity of
124 infection (MOI) of 4 for 72 hrs. Remarkably, the amount of virus detected in the supernatant of
125 culture media by plaque assay differed by as much as 423-fold (Fig. 2B). Immunofluorescence
126 microscopy analyses of ACE2 and SARS-CoV-2 nucleoprotein (NP) in representative monolayers
127 confirmed these findings – SI1 and C1 (susceptible small intestinal and colonic monolayers,
128 respectively, with high *ACE2* transcript levels) displayed higher degrees of ACE2 and NP staining
129 compared with SI10 and C8 (resistant small intestinal and colonic monolayers, respectively) (Fig.
130 2C and D). Indeed, SARS-CoV-2 infection correlated with *ACE2* and *TMRPSS2* expression, but
131 not *TMPRSS4* and *APOA1* expression (Fig. 2E-H). We validated these findings based on relative
132 *ACE2* transcript levels by enumerating absolute RNA copy numbers. The strong correlation
133 between high copy numbers of *ACE2* (2.9×10^5 – 1.7×10^6 transcripts/μg of RNA) with SARS-
134 CoV-2 infection supported the relationship between susceptibility to infection and *ACE2*
135 expression (Supplemental Fig 3D). The amount of virus recovered from monolayers were
136 comparable when the data was segregated by the tissue location, the disease status, or sex of
137 the donors (Supplemental Fig. 3E). Similarly, virus production did not correlate with donor age
138 (Supplemental Fig. 3F).

139 The association between susceptibility to SARS-CoV-2 infection and *ACE2* expression
140 was clear in most cases, but there were outliers for the colonic monolayers. For instance, C7 and
141 C8 have moderate to high levels of ACE2 but low levels of virus production (Fig. 2A and B). Thus,
142 we investigated whether other factors may contribute to differential SARS-CoV-2 infectivity.
143 Several polymorphisms are predicted to alter the stability of ACE2 or alter its affinity to the SARS-
144 CoV-2 spike (S) protein (43-46). However, the sequence of the *ACE2* coding region of C7 and C8
145 were identical to other donors (Supplemental Table 1). Differences in interferon responses may
146 also contribute to SARS-CoV-2 infectivity, where higher ISG levels are predicted to confer
147 protection against viral infection (47-49). Baseline *ISG15*, *OASL*, and *MX2* expression in C7 and
148 C8 did not explain the lower virus production (Supplemental Fig. 3A-C), and we did not observe

149 correlations between *ISG15, OASL*, or *MX2* and SARS-CoV-2 susceptibility (Supplemental Fig.
150 3G-I). Next, we examined ISG expression following stimulation with interferon-beta (IFNβ) or
151 interferon-lambda 2 (IFNλ2). Although we observed varied levels of ISG induction, they were not
152 associated with reduced viral infection (Supplemental Fig. 4A; Supplemental Table 3). Generally,
153 we did not detect an association between the degree to which these ISGs were induced and
154 properties of the donor tissue location, disease status, and age (Supplemental Fig. 4A-C and
155 Supplemental Table 3). However, small intestinal monolayers from female donors displayed
156 higher ISG expression than male donors following IFNλ2 stimulation (Supplemental Fig. 4D).
157 *ACE2* and *TMPRSS2* expression were not altered by IFNβ or IFNλ2 (Supplemental Fig. 5),
158 indicating that *ACE2* and *TMPRSS2* are not ISGs in monolayers. We note that this limited survey
159 of transcript level changes does not rule out a potential role for antiviral cytokines, and a
160 comprehensive protein level analyses of immune mediators will be necessary to identify additional
161 mechanisms of resistance.

162 Our results thus far are consistent with the possibility that *ACE2* gene expression is a key
163 determinant of the degree to which the intestinal epithelium of an individual is susceptible to
164 SARS-CoV-2 infection. As organoids are differentiated from primary stem cells and expanded in
165 culture (50, 51), it was unclear whether inter-donor differences reflect ACE2 levels in the primary
166 tissues. Therefore, we measured ACE2 protein by immunofluorescence microscopy in small
167 intestinal and colonic sections from the same donors corresponding to individual lines of organoid-
168 derived monolayers (Fig. 3 and Supplemental Fig. 6). ACE2 staining was restricted to the
169 epithelium and most intense along the apical brush boarder (villi in the small intestine and top of
170 the crypts in the colon; Fig. 3A and B and Supplemental Fig. 6A and B), consistent with our data
171 and previous studies showing that *ACE2* expression is enriched in differentiated enterocytes (32,
172 33). Primary tissue specimens also displayed heterogeneous ACE2 protein levels (Fig. 3C and
173 Supplemental Fig. 6). The ACE2 mean intensity was decreased in colonic sections of IBD patients,
174 but did not differ when comparing tissue location or sex (Fig 3D). The mean intensity of ACE2
175 staining in intestinal tissue sections strongly correlated with *ACE2* transcript and SARS-CoV-2
176 levels in monolayers derived from the same individual, and not with age, sex, or disease status
177 (Fig. 3E). Therefore, organoid-derived monolayers retain the variable ACE2 levels from its original
178 tissue.

179 To further investigate how susceptible and resistant organoids differ from each other, we
180 selected the three colonic monolayer lines that each displayed high infection (HI; C1, C2, and C3)
181 or low infection (LI; C8, C12, and C13) for RNA-seq analysis. We validated the transcriptional and
182 microscopy analyses (Fig. 2A, C, and D) by Western blot, which showed higher levels of ACE2

183 protein in HI compared with LI monolayers, and comparable levels of TMPRSS2 protein (Fig. 4A).
184 We then infected the monolayers with SARS-CoV-2 for 24 and 72 hrs (I24 and I72, respectively),
185 and compared these samples with mock infected monolayers harvested at 0 and 72 hrs (UI0 and
186 UI72, respectively). SARS-CoV-2 continues to replicate in organoids after the initial 24 hrs, likely
187 due to the low proportion of cells that are initially infected (33). We reasoned sampling early and
188 late time points may distinguish transcriptional changes that contribute to resistance and
189 susceptibility to infection versus those that are a consequence. Because these six monolayer
190 lines were prepared from independently thawed batches of frozen organoid stocks, we quantified
191 virus and confirmed that higher amounts of SARS-CoV-2 were recovered from HI compared with
192 LI monolayers at both time points (Fig. 4B and C). Both HI and LI monolayers remained viable
193 following SARS-CoV-2 infection (Supplemental Fig. 7A). Similar to our findings with IFN-
194 stimulated monolayers (Supplemental Fig. 5), *ACE2* and *TMPRSS2* transcripts in both HI and LI
195 monolayers were stable during the course of infection (Supplemental Fig. 7B and C).
196 The number of transcripts displaying > 2-fold changes (adjusted *P*-value < 0.05) in 12
197 pairwise comparisons are summarized in Supplemental Fig. 7D. The conditions that displayed
198 the most differences from one another were those comparing early time points to 72 hrs post-
199 infection. Uninfected samples at 0 and 72 hrs displayed no differences, indicating that the
200 transcriptome of uninfected HI and LI monolayers remained stable over time. This result increased
201 our confidence that monolayers were fully differentiated at the onset of our experiments. Also,
202 few genes displayed differential expression when comparing uninfected HI and LI monolayers.
203 Principal component analysis (PCA) showed that infection at 72 hrs separated samples on PC1
204 and susceptibility to infection (HI versus LI) separated samples on PC2 (Supplemental Fig. 7E).
205 PCA also confirmed observations from the pairwise comparison indicating that uninfected
206 monolayers and those infected for 24 hrs were transcriptionally similar.
207 At the 72 hr time point, where the largest transcriptional changes occurred between
208 conditions, we found that the majority of the differentially expressed genes (DEGs) when
209 comparing uninfected and infected conditions (55 of 71) were common to LI and HI monolayers,
210 while most DEGs (65 of 81) when comparing infected HI and LI monolayers were unique to this
211 comparison (Fig. 4D). Gene ontology analyses and Ingenuity Pathway Analysis (IPA) showed
212 that SARS-CoV-2 infection impacts antiviral pathways, especially those related to the interferon
213 response, and that this signature was more pronounced in HI monolayers compared with LI
214 monolayers following infection (Fig. 4E-G and Supplemental Fig. 7F). Indeed, differentially
215 expressed genes related to the *response to type I IFN* (*SAMHD1*, *NLRC5*, *USP18*, *IFIT1*, *ZBP1*,
216 *SHFL*, *STAT2*, *IRF7*, *SP100*, *MX1*, *OAS3*, *STAT1*, *ISG15*, and *OAS2*) and *JAK-STAT* (*STAT5A*,

217 *STAT1*, *STAT2*, *CCL2*, and *NMI*) included common ISGs, and although these were upregulated
218 in both HI and LI monolayers infected by SARS-CoV-2, they were induced to a higher degree in
219 HI monolayers (Supplement Fig. 7G and H). Because these ISGs are more highly expressed in
220 HI monolayers and not detected at 24 hrs, they are likely a response to the increased degree of
221 infection. These results are consistent with other studies suggesting that the interferon response
222 to SARS-CoV-2 is delayed (33, 49, 52, 53). Unexpectedly, multiple genes associated with
223 pathways related to zinc and copper homeostasis were specifically upregulated in LI compared
224 to HI monolayers after 72 hrs of infection (Fig 4E, H and Supplemental Fig. 7I). The increased
225 expression of *MT1* genes encoding metallothionines in LI monolayers was particularly striking
226 and may be indicative of a stress response activated by viral perturbations in the epithelium (54,
227 55). Collectively, longitudinal transcriptome analyses identified robust yet late transcriptional
228 changes induced by SARS-CoV-2, the magnitude of which corresponded to the levels of viral
229 infection.

230 The transcriptome analysis did not provide additional insight into the difference in *ACE2*
231 between expression displayed by HI and LI monolayers. The transcription factors BRG1, FOXM1,
232 and FOXA2 mediate *ACE2* expression (56, 57) but consistent with the RNA-Seq results, HI and
233 LI monolayers displayed comparable *BRG1*, *FOXM1*, and *FOXA2* expression by qPCR
234 (Supplemental Fig. 8A-C). However, we detected increased protein levels of FOXA2 in HI
235 monolayers by Western blot, suggesting a probable mechanism for the high *ACE2* expression
236 observed in these donors (Supplemental Fig. 8D).

237 During the preparation of this manuscript, a new variant of concern designated as
238 Omicron emerged with multiple amino acid substitutions in the S protein. Thus, we examined the
239 ability of the Omicron S protein to mediate entry into intestinal epithelial cells using SARS-CoV-2
240 S protein-pseudotyped lentiviral reporter viruses (58). Vesicular stomatitis virus G protein (VSV-
241 G) pseudotyped control virus displayed high infectivity of organoid-derived monolayers
242 demonstrating feasibility of this approach (Supplemental Fig. 9A). Although Omicron S protein
243 has been observed to have weaker or comparable binding affinity to ACE2 (59, 60), Omicron S
244 protein pseudotyped virus displayed 2.5- and 5-fold higher infection than Delta and D614G
245 pseudotypes, respectively (Supplemental Fig. 9A), suggesting that Omicron exploits different or
246 additional cell entry pathways to replicate in human intestinal organoids. Consistent with our
247 observation, a recent study showed efficient entry of Omicron using the endosomal route (61).
248 D614G and Omicron S protein pseudotyped viruses showed 1.2- to 1.3-fold higher infection of HI
249 monolayers compared with LI monolayers whereas the Delta S protein pseudotyped virus
250 displayed comparable infectivity (Supplemental Fig. 9B). This marginal contribution of the

251 differential *ACE2* expression to infection of these pseudotyped viruses suggests that other factors
252 may be involved in SARS-CoV-2 susceptibility of intestinal epithelial cells. For example, *MT1*
253 genes identified in our RNA-Seq experiment (Fig. 4E and H) are associated with resistance to
254 hepatitis C virus and human cytomegalovirus, and zinc ion suppresses the SARS-CoV-2
255 replications by inhibiting its main proteases (62-65). Although we caution against overinterpreting
256 these results obtained with pseudotyped viruses, we believe these preliminary results justify future
257 studies using intestinal organoids and other donor-derived cell culture systems to examine
258 differential susceptibility to intact viruses representing existing and future variants.
259 When taken together, our results show that human intestinal organoids reveal
260 interindividual differences in responses to viral infection. Organoid-derived monolayers showed
261 substantial differences in their susceptibility to SARS-CoV-2 infection, and ACE2 levels were the
262 strongest correlate of susceptibility. Although transcriptome analysis identified many differentially
263 expressed genes upon SARS-CoV-2 infection when comparing organoid lines, these differences
264 were not apparent at 24 hrs post-infection, a time point at which the degree of virus infection
265 already diverged between resistant and susceptible monolayers. Therefore, these gene
266 expression patterns are unlikely to account for differential susceptibility, and instead, provide a
267 glimpse as to how increased viral replication can affect properties of the intestinal epithelium.
268 Although the presence of SARS-CoV-2 RNA in the gut has been associated with diarrhea in
269 patients with COVID-19 (27), the consequence of intestinal epithelial infection remains largely
270 unclear and an important area of investigation. Extensive experiments in animal models predict
271 that activation of viral RNA sensors trigger immune responses including ISGs that impact the
272 intestinal barrier (66-76). Co-culturing organoids with leukocytes may help our understanding of
273 the downstream consequences of epithelial infections (7). Additionally, loss of microbiome
274 diversity is associated with COVID-19 severity (77-80). It would be important to determine whether
275 the microbiome is involved in infection of the epithelium or represents an independent variable of
276 disease outcome.
277 Finally, it is notable that organoids retained the differential ACE2 levels observed in intact
278 primary tissue sections from the same donor. These results indicate that at least some
279 transcriptional properties of the original intestinal epithelium that are individual-specific are
280 retained following *ex vivo* differentiation. If this finding is generalizable, then organoids can be a
281 powerful platform to investigate interindividual differences in infectious disease susceptibility.
282

283 **METHODS**

284 **Human intestinal tissue specimen collection:**

285 Patients with and without IBD were recruited at outpatient colonoscopy performed for colon
286 cancer screening, surveillance, or IBD activity assessment at NYU Langone Health's
287 Ambulatory Care Center, New York, under an NYU Grossman School of Medicine Institutional
288 Review Board–approved study (Mucosal Immune Profiling in Patients with Inflammatory Bowel
289 Disease; S12-01137). Approximately 6 pinch biopsies were obtained from the ascending colon
290 of each patient using a 2.8-mm standard endoscopic biopsy forceps. The inflammation status
291 of tissue was confirmed by endoscopic and histopathological examination. All pinch biopsies
292 were collected in ice-cold complete RPMI (RPMI 1640 medium supplemented with 10% fetal
293 bovine serum (FBS), penicillin/streptomycin/glutamine, and 50 μM 2-mercaptoethanol). Pinch
294 biopsies were then transferred to freezing media (90% FBS + 10% DMSO) in Cryogenic Tubes
295 and stored in liquid nitrogen.

296

297 **Culture of human small intestinal and colonic organoids:**

298 Human organoids were cultured as described previously (7, 68). Pinch biopsies were thawed in
299 PBS and then incubated in Gentle Cell Dissociation Reagent (Stemcell Technologies) on ice for
300 30 min, followed by vigorous pipetting to isolate crypts. The crypts were embedded in 30 μl of
301 Matrigel and cultured with Human IntestiCult™ Organoid Growth Medium (OGM) (Basal Medium
302 and Organoid Supplement, Stemcell Technologies) supplemented with 100 IU Penicillin and 100
303 μg/ml Streptomycin (Corning) and 125 μg/ml Gentamicin (ThermoFisher), herein referred to as
304 expansion medium. The culture medium was changed every 2-3 days. For passaging human
305 organoids, 10 μM Y-27632 were added for the first 2 days. For differentiation, the human
306 organoids were cultured with 1:1 mix of Human IntestiCult™ OGM Basal Medium and DMEM/F-
307 12 (ThermoFisher) in the presence of 100 IU Penicillin and 100 μg/ml Streptomycin, 125 μg/ml
308 Gentamicin and 2 mM L-Glutamine (Corning), herein referred to as differentiation medium. To
309 generate organoid-derived monolayers, mature human small intestinal colonic organoids grown
310 with the expansion media were digested into single cells using TrypLE Express (ThermoFisher)
311 and seeded into Matrigel-coated 96-well culture plate (Corning) in Y-27632-supplemented
312 expansion medium at 150,000 cells/well for the first 2 days. The culture media were changed
313 every day. In experiments in which organoids were treated with recombinant interferons,
314 monolayers grown with the differentiation media for 7 days were stimulated with human IFNβ (100
315 or 300 IU/ml, R&D systems) or IFNλ2 (10 or 30 ng/ml, R&D systems) for 12 hrs.

316 **Transcript analysis:**

317 Total RNA was extracted from human organoids using RNeasy Mini Kit with DNase treatment
318 (QIAGEN), and synthesis of cDNA was conducted with High-Capacity cDNA Reverse
319 Transcription Kit (ThermoFisher) according to the manufacturer's protocol. RT-PCR was
320 performed using SybrGreen (Roche) on a Roch480II Lightcycler using the following primers:
321 *ACE2*, Fwd 5'-TCAAGGAGGCCGAGAAGTTC-3' and Rev 5'-TTCCTGGGTCCGTTAGCATG-3';
322 *TMPRSS2*, Fwd 5'-ACCTGATCACACCAGCCATG-3' and Rev 5'-
323 CTTCGAAGTGACCAGAGGCC-3'; *TMPRSS4*, Fwd 5'-CCGATGTGTTCAACTGGAAG-3' and
324 Rev 5'-GAGAAAGTGAGTGGGAACTG-3'; *APOA1*, Fwd 5'-TGGATGTGCTCAAAGACAGC-3'
325 and Rev 5'-AGGCCCTCTGTCTCCTTTTC-3'; *ISG15*, Fwd 5'-GAGAGGCAGCGAACTCATCT-3'
326 and Rev 5'-CTTCAGCTCTGACACCGACA-3'; *OASL*, Fwd 5'-AAAGAGAGGCCCATCATCC-3'
327 and Rev 5'-ATCTGGGTAACCCCTCTG C-3'; *MX2*, Fwd 5'-CAGCCACCACCAGGAAACA-3' and
328 Rev 5'-TTCTGCTCGTACTGGCTGTACAG-3'; BRG1, Fwd 5'-AGTGCTGCTGTTCTGCCAAAT-3'
329 and Rev 5'-GGCTCGTTGAAGGTTTTCAG-3'; FOXM1, Fwd 5'-GCAGGCTGCACTATCAACAA-
330 3' and Rev 5'-TCGAAGGCTCCTCAACCTTA-3'; FOXA2, Fwd 5'-GGGAGCGGTGAAGATGGA-
331 3' and Rev 5'-TCATGTTGCTCACGGAGGAGTA-3'; *GAPDH*, Fwd 5'-GATGGGATTTCCATTGAT
332 GACA-3' and Rev 5'-CCACCCATGGCAAATTCC-3'; ACTB, Fwd 5'-
333 CCCAGCCATGTACGTTGCTA-3' and Rev 5'-TCACCGGAGTCCATCACGAT-3'; SARS-CoV-2
334 NP, Fwd 5'- ATGCTGCAATCGTGCTACAA-3'; SARS-CoV-2 N, Rev 5'-
335 GACTGCCGCCTCTGCTC-3'. The expression of the respective genes was normalized by
336 geometric mean of *GAPDH* and *ACTB* expression with $\Delta\Delta C_T$ method (81). Where indicated, the
337 values were expressed as fold change from uninfected or untreated organoids. To determine the
338 copy number of *ACE2* mRNA, a standard curve was constructed with the range of 1.4×10^5 to
339 9.4×10^9 molecules of hACE2 (Plasmid #1786, Addgene) (82) in which *ACE2* transcripts showed
340 optimal PCR efficiencies. The copy number of *ACE2* transcripts in the organoids was calculated
341 from the linear regression of the standard curve and normalized with the RNA input.

342

343 **Virus infection and plaque assay:**

344 SARS-CoV-2 infection experiments were performed in the ABSL3 facility of NYU Grossman
345 School of Medicine in accordance with its Biosafety Manual and Standard Operating
346 Procedures. The organoid monolayers grown with the differentiation media for 7 days were
347 infected with icSARS-CoV-2-mNG (isolate USA/WA/1/2020) obtained from the UTMB World
348 Reference Center for Emerging Viruses and Arboviruses (83). A working stock of SARS-CoV-
349 2-mNG was generated by infecting a 90-95% confluent monolayer of Vero E6 cells (ATCC CRL-

350 1586) for 48 hrs at 37°C. Following incubation, the supernatant was collected, centrifuged at
351 1,200 rpm for 5 mins, aliquoted and stored at -80°C. Viral titers were quantified by plaque assay
352 as described below. For the infection, organoid monolayers were infected with SARS-CoV-2-
353 mNG at a MOI of 4 for 1 hr at 37°C. Following incubation, organoids were washed 4 times with
354 phosphate buffered saline (PBS) and differentiation media was added for the indicated time.
355 Total virus in the 3rd or 4th wash was also quantified to ensure excess virus was removed. Thus,
356 virus quantified at the end of the experiment can be assessed as replicative particles rather than
357 residual particles persisting in culture. Viral titers in the monolayer supernatants were quantified
358 by plaque assay.

359 To quantify infectious virus by plaque assay, 10-fold serial dilutions of each sample
360 were made in Dulbecco's Modified Eagle Medium (DMEM). Each dilution was added to a
361 monolayer of Vero E6 cells for 1 hr at 37°C. Following incubation, DMEM supplemented with
362 2% fetal bovine serum and 0.8% agarose was added and the incubated for 72 hrs at 37°C. Cells
363 were then fixed with 10% formalin, the agarose plug removed, and wells stained with crystal
364 violet (10% crystal violet, 20% ethanol). Virus titers (PFU/ml) were determined by counting the
365 number of plaques on the lowest countable dilution.

366 For thiazolyl blue tetrazolium bromide (MTT) reduction assay, staining with MTT was
367 adapted from a previously described method (7). Briefly, we added MTT (Sigma-Aldrich) into the
368 monolayers to a final concentration of 500 µg/ml on 72 hrs post-infection. After incubation for 2
369 hrs at 37°C, 5% CO_2, the medium was discarded and 20 µl of 2% SDS (Sigma-Aldrich) solution
370 in water was added to solubilize the Matrigel for 2 hrs. Then, 100 µl of DMSO (ThermoFisher)
371 was added for 1 hr to solubilize the reduced MTT, and OD was measured on a microplate
372 absorbance reader (ParkinElmer) at 562 nm. The specific organoid death (%) was calculated as
373 MTT deduction (%) by normalizing to uninfected monolayers which were defined as 100% viable.
374

375 ***ACE2* sequencing:**

376 A 2418-bp region containing the *ACE2* coding region was amplified from cDNA prepared from
377 organoids (see above) by PCR using a pair of primers (Fwd 5'-ATGTCAAGCTCTTCCTGGCTCC-
378 3' and Rev 5'-CTAAAAGGAGGTCTGAACATCATCAGTG-3'). Amplicons were cloned into
379 pCR™2.1-TOPO® (Invitrogen). The plasmids were sequenced by Sanger sequencing from
380 Psomagen using 4 primers: M13F, 5'-GTAAAACGACGGCCAGT-3'; M13R, 5'-
381 CAGGAAACAGCTATGAC-3'; ACE2_600F, 5'- GGGGATTATTGGAGAGGAGACT-3';
382 ACE2_1800R, 5'- GTCGGTACTCCATCCCACA-3'.
383

384 **Immunofluorescence:**

385 ACE2 staining were performed as described previously (84). Briefly, pinch biopsies of the terminal
386 ileum and ascending colon were fixed in 10% formalin and embedded in paraffin blocks. Sections
387 were cut to 5 µm thickness at the NYU Center for Biospecimen Research and Development and
388 mounted on frosted glass slides. For deparaffinization, slides were baked at 70°C for 1.5 h,
389 followed by rehydration in descending concentration of ethanol (100%, 95%, 80%, 70%, ddH_2O
390 twice; each step for 30 s). HIER was performed in a pressure cooker (Biocare Medical) using
391 Dako Target Retrieval Solution, pH 9 (Dako Agilent) at 97°C from 10 min and cooled down to
392 65°C. After further cooling to room temperature for 20 min, slides were washed for 10 min 3 times
393 in Tris-Buffered Saline (TBS), containing 0.1% Tween 20 (Sigma; TBS-T). Sections were blocked
394 in 5% normal donkey serum (Sigma) in TBS-T at room temperature (RT) for 1 hr, followed by
395 incubation with rabbit anti-ACE2 antibody (1:100, Abcam, ab15348) in the blocking solution at
396 4°C overnight. Sections were washed 3 times with TBS-T and stained with the Alexa Flour 555
397 conjugated with donkey anti-rabbit IgG (1:500, ThermoFisher, A-31572) in PBS with 3% bovine
398 serum albumin (BSA) (ThermoFisher), 0.4% saponin, and 0.02% sodium azide at RT for 1 hr.
399 Following this, sections were washed 3 times with TBS-T and mounted with ProLong™ Glass
400 Antifade Mountant with NucBlue™ Stain (ThermoFisher, P36918). Images were acquired using
401 an EVOS FL Auto Cell Imaging System (ThermoFisher) and then processed and quantified using
402 ImageJ.

403 SARS-CoV-2-infected monolayers were fixed with 4% paraformaldehyde (Electron
404 Microscopy Sciences) for 3 hrs at RT. Following fixation, cells were washed 3 times with PBS
405 then blocked and permeabilized in PBS with 0.1% Triton-X100 and 3% BSA for 0.5 hr at RT. The
406 permeabilized organoids were washed 3 times with PBS and incubated with mouse anti-SARS-
407 CoV-2 N antibody (1:1,000, ProSci, 10-605) and rabbit anti-ACE2 antibody (1:500, Abcam,
408 ab15348) diluted in PBS containing 3% BSA overnight at 4°C. The monolayers were washed 3
409 times with PBS and stained with Alexa Flour 647 conjugated with goat anti mouse IgG (1:2,000,
410 ThermoFisher, A32728) and Alexa Flour 594 conjugated with donkey anti rabbit IgG (1:1,000,
411 ThermoFisher, 21207) diluted in PBS with 3% BSA and 4'6-diamidino-2-phenylindole (DAPI) for
412 1 hr at RT. The monolayers were then washed 3 times with PBS and imaged using the CellInsight
413 CX7 High-content Microscope (ThermoFisher).

414

415 **Immunoblotting:**

416 Organoids were processed for immunoblotting as previously described (76). Briefly, monolayers
417 were incubated in lysis buffer (20 mM Tris-HCl (pH 7.4), 150 mM NaCl, 1% Triton X-100, 10%

418 glycerol, and 2x Halt Protease and Phosphatase Inhibitor Cocktail (ThermoFisher) on ice for 5
419 min and centrifuged at 14,000 rpm for 20 min. Samples were resolved on Bolt 4-12% Bis-Tris
420 Plus Gels (Invitrogen), transferred onto PVDF membranes, and blocked using 5% skim milk.
421 The following antibodies were used for immunoblotting studies: mouse anti-β-actin (1:5,000,
422 Sigma, AC-15), rabbit anti-ACE2 (1:1,000, Abcam, ab15348), mouse anti-TMPRSS2 (1:1,000,
423 Santa Cruz, sc-515727), rabbit anti-BRG1 (1:250, R&D systems, MAB5738), mouse anti-
424 FOXM1 (1:100, Santa Cruz, sc-271746), rabbit anti-FOXA2 (1:200, Cell Signaling Technology,
425 8186). Secondary antibodies (mouse anti-rabbit and goat-anti mouse, 211-032-171 and 115-
426 035-174, respectively) were purchased from JacksonImmunoResearch
427

428 **RNA deep sequencing and analysis:**

429 Monolayers were cultured in differentiation media for 7 days and then were infected with SARS-
430 CoV-2 at MOI of 4 for 24 hrs or 72 hrs before RNA extraction with 2-3 technical duplicates per
431 line. CEL-seq2 was performed on 53 human organoids RNA samples. Sequencing was
432 performed on Illumina NovaSeq 6000 (Illumina). RNA-seq results were processed using the R
433 package "DESeq2" to obtain variance stabilized count reads, fold changes relative to specific
434 condition, and statistical *P*-value. Analysis of the organoid transcriptome focused on
435 differentially expressed genes, defined as the genes with an absolute fold change relative to
436 specific condition >2 and an adjusted *P*-value < 0.05.
437

438 **Plasmids**

439 SARS-CoV-2 S expression vectors have been previously described (58). Briefly, the SARS-
440 CoV-2 S expression vector pcCoV2.S.Δ19, *S* gene was amplified from pcCOV2.S (Wuhan-Hu-
441 1/2019 SARS-CoV-2 isolate) (58) with a forward primer containing Kpn-I site and reverse primer
442 that deleted the 19 carboxy-terminal amino acids and contained Xho-I site. The amplicon was
443 then cloned into the Kpn-I and Xho-I of pcDNA6 (invitrogen). The D614G mutation was
444 introduced by overlap extension PCR of the Δ19.*S* gene using internal primers overlapping the
445 D614G mutation and cloned into pcDNA6. Mutations in Delta variant S were introduced by
446 overlapping PCR overlapping each Delta mutations and cloned into pcDNA6. The Omicron S
447 expression vector was chemically synthesized and cloned into pcDNA6 (85). pcVSV-G,
448 pLenti.GFP.NLuc, lentiviral packaging plasmids pMDL and pRSV.Rev have been previously
449 described (58).
450

451 **SARS-CoV-2 S lentiviral pseudotypes**

452 SARS-CoV-2 variant S protein pseudotyped lentiviral stocks were generated by cotransfection
453 of 293T cells (4 X 10^6) with pMDL, pLenti.GFP-NLuc, pcCoV2.S.Δ19 and pRSV.Rev (4:3:4:1
454 mass ratio) by calcium phosphate coprecipitation as previously described (58). VSV-G
455 pseudotyped lentivirus was generated substituting the S protein vector for pcVSV-G. Two days
456 post-transfection, supernatant was harvested and passed through a 0.45 μm filter and
457 ultracentrifuged over a 20% sucrose cushion at 30,000 RPM for 90 min. The virus pellet was
458 resuspended to 1/10 the initial volume in DMEM with 10% FBS and virus titers were normalized
459 by real-time PCR reverse transcriptase activity. Pseudotyped virus infectivity assay was done
460 with HI and LI monolayers at an MOI of 0.2. After 72 hrs of infection, luciferase activity was
461 measured by Nano-Glo luciferase substrate (Promega) with an Envision 2103 microplate
462 luminometer (PerkinElmer).

463

464 **Computational and statistical analysis**

465 Gene ontology analysis was performed using the R package "clusterProfiler". Principal
466 Component Analysis was performed using the R package "stats". Heatmaps were generated
467 using the R package "pheatmap". Upstream regulators analysis was performed by uploading
468 the differentially expressed genes to Ingenuity Pathway Analysis software (Qiagen). Statistical
469 differences were determined as described in figure legend using either R or GraphPad Prism 9
470 software (La Jolla, CA, USA).

471

472 **Data availability**

473 The accession number for the gene expression raw data reported in this paper is GSE179949.

474

475

FUNDING

This research was supported by NIH grants DK093668 (K.C.), AI121244 (K.C.), HL123340 (K.C.), AI130945 (K.C.), AI140754 (K.C.), DK124336 (K.C.), DA046100 (N.R.L), AI122390 (N.R.L), and AI120898 (N.R.L) and a pilot award from the NYU CTSA grant UL1TR001445 from the National Center for Advancing Translational Sciences (NCATS) (K.C.). Additional support was provided by the Faculty Scholar grant from the Howard Hughes Medical Institute (K.C.), Crohn's & Colitis Foundation (K.C.), Kenneth Rainin Foundation (K.C.), Judith & Stewart Colton Center of Autoimmunity (K.C.). K.C. is a Burroughs Wellcome Fund Investigator in the Pathogenesis of Infectious Diseases. M.E.K was supported by a Public Health Service Institutional Research Training Award T32 AI7647.

DECLARATION OF INTERESTS

K.C. has received research support from Pfizer, Takeda, Pacific Biosciences, Genentech, and Abbvie. K.C. has consulted for or received an honoraria from Puretech Health, Genentech, and Abbvie. K.C. holds U.S. patent 10,722,600 and provisional patent 62/935,035 and 63/157,225.

ACKNOWLEDGMENTS

We wish to thank the NYU Grossman School of Medicine Center for Biospecimen Research and Development, Office of Science & Research High-Containment Laboratories, and Flow Cytometry and Cell Sorting, Microscopy, Genome Technology, and Histology Cores (supported by National Institutes of Health [NIH] grants P31CA016087, S10OD01058, and S10OD018338) for their support in the completion of this research and Dr. Meike Dittmann at the NYU Grossman School of Medicine for use of the CX7 CellInsight high-content microscope.

AUTHOR CONTRIBUTION

Conceptualization: Kyung Ku Jang, Kenneth Stapleford, Ken Cadwell
Data curation: Kyung Ku Jang, Kenneth Stapleford, Ken Cadwell
Formal analysis: Kyung Ku Jang, Maria E Kaczmarek, Ying-Han Chen, Simone Dallari
Funding acquisition: Kenneth Stapleford, Ken Cadwell
Investigation: Kyung Ku Jang, Maria E Kaczmarek, Ying-Han Chen, Simone Dallari, Takuya Tada, Kenneth Stapleford
Methodology: Kyung Ku Jang, Maria E Kaczmarek, Ying-Han Chen, Simone Dallari, Takuya Tada, Kenneth Stapleford
Project administration: Kenneth Stapleford, Ken Cadwell
Resources: Kyung Ku Jang, Maria E Kaczmarek, Ying-Han Chen, Simone Dallari, Jordan Axelrad, Nathaniel R. Landau
Supervision: Kenneth Stapleford, Ken Cadwell
Validation: Kyung Ku Jang, Maria E Kaczmarek, Ying-Han Chen, Simone Dallari
Visualization: Kyung Ku Jang, Maria E Kaczmarek, Simone Dallari
Writing – original draft: Kyung Ku Jang, Simone Dallari, Jordan Axelrad, Takuya Tada, Nathaniel R. Landau, Kenneth Stapleford, Ken Cadwell
Writing – review & editing: Kyung Ku Jang, Maria E Kaczmarek, Ying-Han Chen, Simone Dallari, Takuya Tada, Jordan Axelrad, Nathaniel R. Landau, Kenneth Stapleford, Ken Cadwell

521 **Figure 1. Heterogeneous gene expression patterns in small intestinal and colonic**
522 **organoids.**
523 **(A-D)** Correlation analysis of *ACE2* and *TMPRSS2* (A), *TMPRSS4* and *APOA1* (B), *ISG15* and
524 *OASL* (C), or *MX2* (D) expression in human intestinal (circle) and colonic (rectangle) organoids
525 cultured as monolayers grown in differentiation media for 7 days with those cultured as human
526 3D organoids grown in differentiation media (3DD) for 7 days. **(E-K)** RT-PCR data comparing
527 *ACE2* (E), *TMPRSS2* (F), *TMPRSS4* (G), *APOA1* (H), *ISG15* (I), *OASL* (J), and *MX2* (K)
528 expression in human 3D organoids grown with expansion media (3DE), 3DD, and monolayers
529 grown in differentiation media for 7 days. Data points are mean of at least 2 technical replicates
530 of individual organoid lines. Bars represent mean ± SEM, and at least 2 independent experiments
531 were performed. r, Pearson correlation coefficient. $^{**}P \leq 0.01$, $^{***}P \leq 0.001$, and $^{****}P \leq 0.0001$
532 by simple regression analysis in A-D and paired *t* test, two tailed in E-K.
533
534 **Figure 2. Differential susceptibility of intestinal organoid-derived monolayers correlates**
535 **with *ACE2* and *TMPRSS2* expression.**
536 **(A)** RT-PCR analysis of *ACE2* expression in small intestinal (SI1-SI12) and colonic (C1-C13)
537 monolayers. **(B)** Plaque forming units (PFU) determined by virus titration on Vero E6 cells of
538 supernatant from monolayers at 72 hrs post-infection with SARS-CoV-2. **(C)** Representative
539 immunofluorescence microscopy images showing co-staining of DAPI (blue), ACE2 (green), and
540 SARS-CoV-2 nucleoprotein (NP) (red) in SARS-CoV-2 infected SI1, SI10, C1, and C8 monolayer
541 lines. An image of uninfected C1 is shown as a representative uninfected condition and a Matrigel-
542 coated well without cells is shown as a control for background fluorescence. **(D)** Total intensity of
543 NP and ACE2 normalized with cell counts of SI1, SI10, C1 and C8. **(E-H)** Correlation of SARS-
544 CoV-2 PFU with *ACE2* (E), *TMPRSS2* (F), *TMPRSS4* (G), or *APOA1* (H) expression among
545 monolayers. Data points in A, B, and D are each technical replicate, and data points in E-H are
546 the mean of at least 2 technical replicates of individual organoid lines. Bars represent mean ±
547 SEM, and at least 2 independent experiments were performed. r, Pearson correlation coefficient.
548 $^{*}P \leq 0.05$, $^{**}P \leq 0.01$, $^{***}P \leq 0.001$, and $^{****}P \leq 0.0001$ by simple regression analysis in E-H.
549
550 **Figure 3. Differential *ACE2* expression observed in individual intestinal organoid lines are**
551 **conserved in primary tissue from the same donor.**
552 **(A and B)** Representative ACE2 staining images in primary tissues of terminal ileum (A) and
553 ascending colon (B) from which SI1, SI10, C1, and C13 organoids were established. **(C)** Mean
554 intensity of ACE2 per area (right) in each field of view from the primary tissues from which small

555 intestinal and colonic organoids were established. **(D)** Mean intensity of ACE2 by disease (left) or
556 sex (right). **(E)** Correlation of ACE2 mean intensity with *ACE2* expressions (left) and SARS-CoV-
557 2 PFU (middle) among monolayers or subject age (right). Data points in C are the field of views,
558 and data points in D and E are mean of at least 2 technical replicates of individual organoid lines.
559 Bars represent mean ± SEM, and at least 2 independent experiments were performed. Bars: 200
560 μm. SI, small intestine; r, Pearson correlation coefficient. *$P \leq 0.05$, **$P \leq 0.01$, ***$P \leq 0.001$, and
561 ****$P \leq 0.0001$ by unpaired *t* test, two-tailed in D and simple regression analysis in E.
562
563 **Figure 4. Transcriptome analysis reveals a heighted and delayed interferon response to**
564 **SARS-CoV-2 infection in susceptible organoid-derived monolayers.**
565 **(A)** Western blot analysis of ACE2, TMPRSS2, and ACTB in high infection (HI; C1, C2, and C3)
566 and low infection (LI; C8, C12, and C13) lines. Blots are representative of at least 3 independent
567 repeats. **(B)** PFU determined by virus titration on Vero E6 cells of supernatant of HI and LI
568 monolayers at 24 and 72 hrs after infection with SARS-CoV-2. **(C)** RT-PCR analysis of SARS-
569 CoV-2 expression in HI and LI monolayers upon 24 and 72 hrs infection with SARS-CoV-2. **(D)**
570 Venn diagram depicting the number and overlap of differentially expressed genes (DEGs)
571 according to RNA-Seq analysis (see Supplemental Fig. 7) of HI or LI monolayers infected with
572 SARS-CoV-2 for 72 hrs. **(E)** Highly enriched biological process GO terms for the DEGs in HI and
573 LI infected with SARS-CoV-2. **(F and G)** Ingenuity pathway analysis (IPA) of the transcriptome of
574 SARS-CoV-2-infected HI or LI for upstream regulators. Interferon-related genes (F) or Top 5
575 molecules within the classes *cytokine, transcription regulator, transmembrane receptor, ligand-*
576 *dependent nuclear receptor, and others* (G) commonly associated with HI infected/uninfected and
577 LI infected/uninfected conditions. **(H)** DEGs of LI infected/HI infected condition were analyzed by
578 IPA for upstream regulators. Top 5 upstream regulators related to Zn ion homeostasis and
579 interferons for the LI. Data points in B and C represent the mean of at least 2 technical replicates
580 of individual organoids lines. Bars represent mean ± SEM, and at least 2 independent
581 experiments were performed. *$P \leq 0.05$, and **$P \leq 0.01$, by unpaired *t* test, two-tailed in B and C.
582
583 **Supplemental figure 1. Transcriptional analysis in small intestinal and colonic organoids**
584 **cultured in different media conditions.**
585 **(A-D)** RT-PCR analysis of *ACE2* (A), *TMPRSS2* (B), *TMPRSS4* (C), *APOA1* (D), *ISG15* (E),
586 *OASL* (F), and *MX2* (G) expression among small intestinal (SI) or colonic 3D organoids grown in
587 expansion media (3DE) or differentiation media (3DD) for 7 days. **(H)** RT-PCR data showing
588 *ACE2*, *TMPRSS2*, *TMPRSS4*, *APOA*, *ISG15*, *OASL*, and *MX2* expression in 3DE organoids

589 according to disease status. **(I-L)** RT-PCR analysis of *ACE2* (I), *TMPRSS2* (J), *TMPRSS4* (K),
590 and *APOA1* (L) expression among SI and colonic monolayers grown in differentiation media for
591 7 days. Data points are mean of 3 technical replicates of individual organoid lines. Bars represent
592 mean, and at least 2 independent experiments were performed. SI, small intestine. $^{**}P \leq 0.01$,
593 $^{***}P \leq 0.001$, and $^{****}P \leq 0.0001$ by paired *t* test, two-tailed in A-G and unpaired *t* test, two-tailed
594 in H-L.
595
596 **Supplemental figure 2. Transcript analysis of organoid-derived monolayers according to**
597 **tissue location, disease, and sex of subjects.**
598 **(A)** RT-PCR analysis of *ACE2*, *TMPRSS2*, *TMPRSS4*, *APOA1*, *ISG15*, *OASL*, and *MX2*
599 expression between matched donor-derived small intestinal (SI) and colonic monolayers grown
600 in differentiation media for 7 days. Data is displayed fold-change differences between the
601 expression of the indicated genes in colonic monolayers over expression in SI monolayers **(B and**
602 **C)** Correlation of *ACE2* (B) and *TMPRSS2* (C) expression with *APOA1* expression among
603 monolayers grown in differentiation media. **(D)** RT-PCR analysis of *ACE2* expression among
604 monolayers grown in differentiation media according to the disease status or sex of subjects. **(E**
605 **and F)** RT-PCR data depicting *ACE2*, *TMPRSS2*, *TMPRSS4*, *APOA1*, *ISG15*, *OASL*, and *MX2*
606 expression of monolayers according to disease (E) or sex (F). Data points are mean of at least 2
607 technical replicates of individual organoid lines. Bars represent mean ± SEM, and at least 2
608 independent experiments were performed. FC, fold change; SI, small intestine; r, Pearson
609 correlation coefficient. $^{*}P \leq 0.05$, $^{**}P \leq 0.01$, and $^{***}P \leq 0.001$ by paired *t* test, two-tailed in A,
610 simple regression analysis in B and C, and unpaired *t* test, two-tailed in D-F.
611
612 **Supplemental figure 3. Analysis of gene expression and viral replication in organoids by**
613 **intestinal region, disease, sex, or age of subjects.**
614 **(A-C)** RT-PCR analysis of *ISG15* (A), *OASL* (B), and *MX2* (C) expression in monolayers. **(D)**
615 Correlation of ACE2 coly number with ACE2 expression (left) or PFU of SARS-CoV-2 (right). **(E)**
616 PFU of SARS-CoV-2 according to intestinal region (left), disease (middle), or sex (right) of
617 subjects. **(F-I)** Correlation of PFU of SARS-CoV-2 with age of subjects (F) or *ISG15* (G), *OASL*
618 (H), and *MX2* (I) expression. Data points are mean of at least 2 technical replicates of individual
619 organoid lines. Bars represent mean ± SEM, and at least 2 independent experiments were
620 performed. SI, small intestine; r, Pearson correlation coefficient. $^{*}P \leq 0.05$, $^{**}P \leq 0.01$, $^{***}P \leq$
621 0.001, and $^{****}P \leq 0.0001$ by unpaired *t* test, two-tailed in A-C and E and simple regression
622 analysis in D and F-I.

623

624 **Supplemental figure 4. Transcript analysis of IFNβ- or IFNλ2-stimulated organoids**
625 **according to intestinal region, disease status, or sex of subjects.**
626 **(A-E)** RT-PCR data depicting fold change in *ISG15*, *OASL*, and *MX2* expression in small intestinal
627 and colonic monolayers stimulated with IFNβ (100 or 300 IU/ml) or IFNλ2 (10 or 30 ng/ml) for 12
628 hrs according to intestinal region (A), disease status (B and C) or sex (D and E) of subjects. Each
629 value is normalized to non-stimulated organoid lines. Data points are mean of at least 2 technical
630 replicates of individual organoid lines. Bars represent mean ± SEM, and at least 2 independent
631 experiments were performed. SI, small intestine. *$P \leq 0.05$ and **$P \leq 0.01$ by unpaired *t* test, two-
632 tailed.
633

634 **Supplemental figure 5. Stimulation with IFNβ or IFNλ2 does not alter *ACE2* and *TMPRSS2***
635 **expression in organoids.**
636 **(A and B)** RT-PCR depicting *ACE2* (A) and *TMPRSS2* (B) expression in monolayers stimulated
637 with IFNβ (100 or 300 IU/ml) or IFNλ2 (10 or 30 ng/ml) for 12 hrs. Data points are mean of at least
638 2 technical replicates of individual organoid lines. Bars represent mean ± SEM, and at least 2
639 independent experiments were performed. SI, small intestine.
640

641 **Supplemental figure 6. Representative images of ACE2 staining in primary intestinal tissue.**
642 **(A and B)** Representative ACE2 staining images in primary tissues of terminal ileum from which
643 small intestinal (SI2-9 and 12, A) or colonic (C2-9, 11, and 12, B) organoid-derived monolayers
644 were established. Images of remaining monolayers are included in main Figure 3. **(C)**
645 Quantification of the total intensity of ACE2 staining and surface area in each visual field from the
646 primary tissues from which the indicated organoid lines were established. Data points in C are
647 the visual field. Bars in A and B: 200 μm. Bars in C represent mean ± SEM.
648

649 **Supplemental figure 7. Transcriptome and viability of SARS-CoV-2-infected organoids.**
650 **(A)** Viability according to MTT reduction assay of SARS-CoV-2-infected high infection (HI; C1, C2,
651 and C3) and low infection (LI; C8, C12, and C13) lines. **(B and C)** RT-PCR data depicting *ACE2*
652 (B) and *TMPRSS2* (C) expression in HI and LI monolayers with or without SARS-CoV-2 infection.
653 **(D)** Number of up- and down-regulated genes identified by RNA-Seq analysis in the indicated
654 pair-wise comparison of HI and LI monolayer lines at different time point post infection. n = 3
655 organoid lines per group and at least 2 technical replicates per individual organoid line. **(E)**
656 Unsupervised clustering based on expression of most variable genes by organoids lines and
657 infection with SARS-CoV-2 at 24 and 72 hrs. **(F)** Highly enriched molecular function GO terms for

658 the differentially expressed genes (DEGs) in HI and LI infected with SARS-CoV-2 for 72 hrs. **(G**
659 **and H)** Heatmaps displaying normalized expression values of DEGs in HI infected/uninfected and
660 LI infected/uninfected conditions (average fold-change ≥ 2 and adjusted *P*-value ≤ 0.05)
661 annotated in GO:0060338 and GO:0034340 (G) and GO0:07259 (H) **(I)** Heatmap displaying
662 normalized expression values of DEGs in LI infected/HI infected conditions (average fold-change
663 ≥ 2 and adjusted *P*-value ≤ 0.05) annotated in GO:0006882. Data points in A-C are mean of at
664 least 2 technical replicates of individual organoid lines. Bars represent mean ± SEM, and at least
665 2 independent experiments were performed. UI0, uninfected 0 hr; UI72, uninfected 72 hrs; I24,
666 infected for 24 hrs; I72, infected for 72 hrs.
667
668 **Supplemental figure 8. Transcript and Western blot analyses of BRG1, FOXM1, and FOXA2.**
669 **(A-C)** RT-PCR analysis of *BRG1* (A), *FOXM1* (B), and *FOXA2* (C) expression in HI and LI
670 monolayers. **(D)** Western blot analysis of BRG1, FOXM1, FOXA2, and ACTB in HI and LI
671 monolayers. Blots are representative of at least 2 independent repeats. Data points are mean of
672 at least 2 technical replicates of individual organoid lines. Bars represent mean ± SEM, and 2
673 independent experiments were performed. UI0, uninfected 0 hr; UI72, uninfected 72 hrs; I24,
674 infected for 24 hrs; I72, infected for 72 hrs.
675
676 **Supplemental figure 9. Infection of SARS-CoV-2 spike protein-pseudotyped lentiviral**
677 **reporter viruses.**
678 **(A-B)** HI and LI monolayers were infected with VSV-G or SARS-CoV-2 D614G, Delta, or Omciron
679 spike protein pseudotyped viruses at an MOI of 0.2. At 72 hrs post-infection, infectivity was
680 measured by luciferase assay. Data points are mean of at least 2 technical replicates of individual
681 organoid lines. Bars represent mean ± SEM, and 2 independent experiments were performed.
682 RLU, relative luminescence unit. ****$P \leq 0.0001$ by unpaired *t* test, two-tailed.
683

684 **Table S1**

Name	Tissue	Sex	Age	Disease type	Inflammation	ACE2 SNP
SI1	Terminal ileum	M	34	Non-IBD	Non-inflamed	NA
SI2	Terminal ileum	M	24	CD	Non-inflamed	NA
SI3	Terminal ileum	F	47	Non-IBD	Non-inflamed	ND
SI4	Terminal ileum	M	23	CD	Non-inflamed	ND
SI5	Terminal ileum	M	37	CD	Non-inflamed	NA
SI6	Terminal ileum	F	25	Non-IBD	Non-inflamed	NA
SI7	Terminal ileum	M	29	Non-IBD	Non-inflamed	ND
SI8	Terminal ileum	M	47	IBD	Non-inflamed	ND
SI9	Terminal ileum	F	37	CD	Non-inflamed	NA
SI10	Terminal ileum	F	69	CD	Non-inflamed	ND
SI11	Terminal ileum	F	23	Non-IBD	Non-inflamed	NA
SI12	Terminal ileum	M	39	CD	Non-inflamed	NA
C1	Ascending colon	M	34	Non-IBD	Non-inflamed	ND
C2	Ascending colon	M	25	Non-IBD	Non-inflamed	NA
C3	Ascending colon	F	55	UC	Non-inflamed	NA
C4	Ascending colon	F	27	UC	Non-inflamed	NA
C5	Ascending colon	M	29	Non-IBD	Non-inflamed	ND
C6	Ascending colon	M	33	UC	Non-inflamed	NA
C7	Ascending colon	M	33	UC	Non-inflamed	ND
C8	Ascending colon	F	23	Non-IBD	Non-inflamed	ND
C9	Ascending colon	M	24	CD	Non-inflamed	NA
C10	Ascending colon	M	37	CD	Non-inflamed	NA
C11	Ascending colon	F	37	CD	Non-inflamed	NA
C12	Ascending colon	M	21	UC	Non-inflamed	NA
C13	Ascending colon	F	20	UC	Non-inflamed	ND

685

686 **Supplemental Table 1**. Subject information for human endoscopic specimens

687 M; Male, F; Female, CD; Crohn's disease; UC; Ulcerative colitis; SNP, Single nucleotide

688 polymorphism; ND, not detected; NA, not attempted

689

690 **Table S2**

Gene expression	Age					
	SI + Colon		SI		Colon	
	r	*P*	r	*P*	r	*P*
ACE2	-0.056	0.790	-0.329	0.296	0.323	0.282
TMPRSS2	-0.122	0.562	-0.144	0.656	0.068	0.826
TMPRSS4	-0.018	0.931	0.158	0.626	0.320	0.287
APOA1	0.187	0.371	0.041	0.900	-0.235	0.439
ISG15	-0.203	0.330	-0.243	0.446	-0.145	0.636
OASL	0.004	0.985	-0.196	0.541	0.263	0.386
MX2	0.077	0.717	0.157	0.626	-0.018	0.953

691

692 **Supplemental Table 2**. Correlation between subject age and gene expression among the
693 organoid monolayers grown in differentiation media for 7 days. *r*, Pearson correlation coefficient;
694 *P*, *P*-value; SI, small intestine.

695

696 **Table S3**

Gene induction	Age				SARS-CoV-2 replication			
	SI		Colon		SI		Colon	
	r	*P*	*r*	*P*	*r*	*P*	*r*	*P*
ISG15								
100 IU/ml IFNβ	0.384	0.218	0.076	0.806	0.109	0.736	0.146	0.633
300 IU/ml IFNβ	0.311	0.326	0.041	0.894	-0.079	0.806	-0.148	0.630
10 ng/ml IFNλ2	0.433	0.160	-0.206	0.499	-0.071	0.827	-0.131	0.671
30 ng/ml IFNλ2	0.457	0.135	-0.082	0.791	-0.393	0.206	-0.028	0.927
OASL								
100 IU/ml IFNβ	0.835	*0.001****	-0.344	0.250	-0.424	0.169	-0.033	0.916
300 IU/ml IFNβ	0.668	*0.018**	0.103	0.738	-0.300	0.344	-0.096	0.755
10 ng/ml IFNλ2	0.538	0.071	-0.173	0.572	-0.404	0.193	-0.110	-0.720
30 ng/ml IFNλ2	0.623	0.030*	0.430	0.143	-0.274	0.390	-0.163	0.596
MX2								
100 IU/ml IFNβ	-0.250	0.432	-0.102	0.741	0.308	0.331	0.006	0.985
300 IU/ml IFNβ	-0.128	0.691	-0.057	0.853	0.250	0.433	0.015	0.689
10 ng/ml IFNλ2	-0.311	0.326	-0.150	0.626	0.091	0.779	-0.194	0.526
30 ng/ml IFNλ2	0.239	0.454	-0.091	0.768	0.171	0.595	0.013	0.966

697

698 **Supplemental Table 3**. Correlation of subject age or PFU of SARS-CoV-2 with ISG induction in
699 organoids stimulated with IFNβ (100 or 300 IU/ml) or IFNλ2 (10 or 30 ng/ml) for 12 hrs. *r*, Pearson
700 correlation coefficient; *P*, *P*-value; SI, small intestine. *$P \leq 0.05$ and ***$P \leq 0.001$ by simple
701 regression analysis.

702
703

704

705 **References**

706 1. Fujii M, Sato T. Somatic cell-derived organoids as prototypes of human epithelial tissues
707 and diseases. Nat Mater. 2020.
708 2. Geiser P, Di Martino ML, Samperio Ventayol P, Eriksson J, Sima E, Al-Saffar AK, et al.
709 Salmonella enterica Serovar Typhimurium Exploits Cycling through Epithelial Cells To
710 Colonize Human and Murine Enteroids. mBio. 2021;12(1).
711 3. Finkbeiner SR, Zeng XL, Utama B, Atmar RL, Shroyer NF, Estes MK. Stem cell-
712 derived human intestinal organoids as an infection model for rotaviruses. mBio.
713 2012;3(4):e00159-12.
714 4. Hosmillo M, Chaudhry Y, Nayak K, Sorgeloos F, Koo BK, Merenda A, et al. Norovirus
715 Replication in Human Intestinal Epithelial Cells Is Restricted by the Interferon-Induced
716 JAK/STAT Signaling Pathway and RNA Polymerase II-Mediated Transcriptional Responses.
717 mBio. 2020;11(2).
718 5. Drost J, Clevers H. Organoids in cancer research. Nat Rev Cancer. 2018;18(7):407-18.
719 6. Nanki K, Fujii M, Shimokawa M, Matano M, Nishikori S, Date S, et al. Somatic
720 inflammatory gene mutations in human ulcerative colitis epithelium. Nature.
721 2020;577(7789):254-9.
722 7. Matsuzawa-Ishimoto Y, Hine A, Shono Y, Rudensky E, Lazrak A, Yeung F, et al. An
723 intestinal organoid-based platform that recreates susceptibility to T-cell-mediated tissue injury.
724 Blood. 2020;135(26):2388-401.
725 8. Borten MA, Bajikar SS, Sasaki N, Clevers H, Janes KA. Automated brightfield
726 morphometry of 3D organoid populations by OrganoSeg. Sci Rep. 2018;8(1):5319.
727 9. Luo X, Zhou GZ, Zhang Y, Peng LH, Zou LP, Yang YS. Coronaviruses and
728 gastrointestinal diseases. Mil Med Res. 2020;7(1):49.
729 10. Ye L, Yang Z, Liu J, Liao L, Wang F. Digestive system manifestations and clinical
730 significance of coronavirus disease 2019: A systematic literature review. J Gastroenterol
731 Hepatol. 2020.
732 11. D'Amico F, Baumgart DC, Danese S, Peyrin-Biroulet L. Diarrhea During COVID-19
733 Infection: Pathogenesis, Epidemiology, Prevention, and Management. Clin Gastroenterol
734 Hepatol. 2020;18(8):1663-72.
735 12. Gupta A, Madhavan MV, Sehgal K, Nair N, Mahajan S, Sehrawat TS, et al.
736 Extrapulmonary manifestations of COVID-19. Nat Med. 2020;26(7):1017-32.
737 13. Redd WD, Zhou JC, Hathorn KE, McCarty TR, Bazarbashi AN, Thompson CC, et al.
738 Prevalence and Characteristics of Gastrointestinal Symptoms in Patients With Severe Acute
739 Respiratory Syndrome Coronavirus 2 Infection in the United States: A Multicenter Cohort Study.
740 Gastroenterology. 2020;159(2):765-7 e2.
741 14. Cheung KS, Hung IFN, Chan PPY, Lung KC, Tso E, Liu R, et al. Gastrointestinal
742 Manifestations of SARS-CoV-2 Infection and Virus Load in Fecal Samples From a Hong Kong
743 Cohort: Systematic Review and Meta-analysis. Gastroenterology. 2020;159(1):81-95.
744 15. Nobel YR, Phipps M, Zucker J, Lebwohl B, Wang TC, Sobieszczyk ME, et al.
745 Gastrointestinal Symptoms and Coronavirus Disease 2019: A Case-Control Study From the
746 United States. Gastroenterology. 2020;159(1):373-5 e2.
747 16. Aghemo A, Piovani D, Parigi TL, Brunetta E, Pugliese N, Vespa E, et al. COVID-19
748 Digestive System Involvement and Clinical Outcomes in a Large Academic Hospital in Milan,
749 Italy. Clin Gastroenterol Hepatol. 2020;18(10):2366-8 e3.

750 17. Gaebler C, Wang Z, Lorenzi JCC, Muecksch F, Finkin S, Tokuyama M, et al. Evolution
751 of antibody immunity to SARS-CoV-2. Nature. 2021;591(7851):639-44.
752 18. Morone G, Palomba A, Iosa M, Caporaso T, De Angelis D, Venturiero V, et al.
753 Incidence and Persistence of Viral Shedding in COVID-19 Post-acute Patients With Negativized
754 Pharyngeal Swab: A Systematic Review. Front Med (Lausanne). 2020;7:562.
755 19. Park SK, Lee CW, Park DI, Woo HY, Cheong HS, Shin HC, et al. Detection of SARS-
756 CoV-2 in Fecal Samples From Patients With Asymptomatic and Mild COVID-19 in Korea. Clin
757 Gastroenterol Hepatol. 2020.
758 20. Wolfel R, Corman VM, Guggemos W, Seilmaier M, Zange S, Muller MA, et al.
759 Virological assessment of hospitalized patients with COVID-2019. Nature. 2020;581(7809):465-
760 9.
761 21. Holshue ML, DeBolt C, Lindquist S, Lofy KH, Wiesman J, Bruce H, et al. First Case of
762 2019 Novel Coronavirus in the United States. N Engl J Med. 2020;382(10):929-36.
763 22. Guan WJ, Ni ZY, Hu Y, Liang WH, Ou CQ, He JX, et al. Clinical Characteristics of
764 Coronavirus Disease 2019 in China. N Engl J Med. 2020;382(18):1708-20.
765 23. Xiao F, Tang M, Zheng X, Liu Y, Li X, Shan H. Evidence for Gastrointestinal Infection
766 of SARS-CoV-2. Gastroenterology. 2020;158(6):1831-3 e3.
767 24. Coryell MP, Iakiviak M, Pereira N, Murugkar PP, Rippe J, Williams DB, et al. A
768 method for detection of SARS-CoV-2 RNA in healthy human stool: a validation study. Lancet
769 Microbe. 2021.
770 25. Livanos AE, Jha D, Cossarini F, Gonzalez-Reiche AS, Tokuyama M, Aydillo T, et al.
771 Gastrointestinal involvement attenuates COVID-19 severity and mortality. medRxiv. 2020.
772 26. Effenberger M, Grabherr F, Mayr L, Schwaerzler J, Nairz M, Seifert M, et al. Faecal
773 calprotectin indicates intestinal inflammation in COVID-19. Gut. 2020;69(8):1543-4.
774 27. Britton GJ, Chen-Liaw A, Cossarini F, Livanos AE, Spindler MP, Plitt T, et al. SARS-
775 CoV-2-specific IgA and limited inflammatory cytokines are present in the stool of select patients
776 with acute COVID-19. medRxiv. 2020.
777 28. Xiao F, Sun J, Xu Y, Li F, Huang X, Li H, et al. Infectious SARS-CoV-2 in Feces of
778 Patient with Severe COVID-19. Emerg Infect Dis. 2020;26(8):1920-2.
779 29. Bradley BT, Maioli H, Johnston R, Chaudhry I, Fink SL, Xu H, et al. Histopathology
780 and ultrastructural findings of fatal COVID-19 infections in Washington State: a case series.
781 Lancet. 2020;396(10247):320-32.
782 30. Ziegler CGK, Allon SJ, Nyquist SK, Mbano IM, Miao VN, Tzouanas CN, et al. SARS-
783 CoV-2 Receptor ACE2 Is an Interferon-Stimulated Gene in Human Airway Epithelial Cells and
784 Is Detected in Specific Cell Subsets across Tissues. Cell. 2020;181(5):1016-35 e19.
785 31. Muus C, Luecken MD, Eraslan G, Sikkema L, Waghray A, Heimberg G, et al. Single-
786 cell meta-analysis of SARS-CoV-2 entry genes across tissues and demographics. Nat Med.
787 2021;27(3):546-59.
788 32. Zang R, Gomez Castro MF, McCune BT, Zeng Q, Rothlauf PW, Sonnek NM, et al.
789 TMPRSS2 and TMPRSS4 promote SARS-CoV-2 infection of human small intestinal
790 enterocytes. Sci Immunol. 2020;5(47).
791 33. Lamers MM, Beumer J, van der Vaart J, Knoops K, Puschhof J, Breugem TI, et al.
792 SARS-CoV-2 productively infects human gut enterocytes. Science. 2020;369(6499):50-4.
793 34. Zhou J, Li C, Liu X, Chiu MC, Zhao X, Wang D, et al. Infection of bat and human
794 intestinal organoids by SARS-CoV-2. Nat Med. 2020;26(7):1077-83.

795 35. Stanifer ML, Kee C, Cortese M, Zumaran CM, Triana S, Mukenhirn M, et al. Critical
796 Role of Type III Interferon in Controlling SARS-CoV-2 Infection in Human Intestinal Epithelial
797 Cells. Cell Rep. 2020;32(1):107863.
798 36. Vuille-Dit-Bille RN, Liechty KW, Verrey F, Guglielmetti LC. SARS-CoV-2 receptor
799 ACE2 gene expression in small intestine correlates with age. Amino Acids. 2020;52(6-7):1063-
800 5.
801 37. Penninger JM, Grant MB, Sung JJY. The Role of Angiotensin Converting Enzyme 2 in
802 Modulating Gut Microbiota, Intestinal Inflammation, and Coronavirus Infection.
803 Gastroenterology. 2021;160(1):39-46.
804 38. Potdar AA, Dube S, Naito T, Li K, Botwin G, Haritunians T, et al. Altered Intestinal
805 ACE2 Levels Are Associated With Inflammation, Severe Disease, and Response to Anti-
806 Cytokine Therapy in Inflammatory Bowel Disease. Gastroenterology. 2021;160(3):809-22 e7.
807 39. Suarez-Farinas M, Tokuyama M, Wei G, Huang R, Livanos A, Jha D, et al. Intestinal
808 Inflammation Modulates the Expression of ACE2 and TMPRSS2 and Potentially Overlaps With
809 the Pathogenesis of SARS-CoV-2-related Disease. Gastroenterology. 2021;160(1):287-301 e20.
810 40. Triana S, Metz-Zumaran C, Ramirez C, Kee C, Doldan P, Shahraz M, et al. Single-cell
811 analyses reveal SARS-CoV-2 interference with intrinsic immune response in the human gut. Mol
812 Syst Biol. 2021;17(4):e10232.
813 41. Zhang H, Li HB, Lyu JR, Lei XM, Li W, Wu G, et al. Specific ACE2 expression in
814 small intestinal enterocytes may cause gastrointestinal symptoms and injury after 2019-nCoV
815 infection. Int J Infect Dis. 2020;96:19-24.
816 42. Potdar AA, Dube S, Naito T, Botwin G, Haritunians T, Li D, et al. Reduced expression
817 of COVID-19 host receptor, ACE2 is associated with small bowel inflammation, more severe
818 disease, and response to anti-TNF therapy in Crohn's disease. medRxiv. 2020.
819 43. Lanjanian H, Moazzam-Jazi M, Hedayati M, Akbarzadeh M, Guity K, Sedaghati-Khayat
820 B, et al. SARS-CoV-2 infection susceptibility influenced by ACE2 genetic polymorphisms:
821 insights from Tehran Cardio-Metabolic Genetic Study. Sci Rep. 2021;11(1):1529.
822 44. Guo X, Chen Z, Xia Y, Lin W, Li H. Investigation of the genetic variation in ACE2 on
823 the structural recognition by the novel coronavirus (SARS-CoV-2). J Transl Med.
824 2020;18(1):321.
825 45. Calcagnile M, Forgez P, Iannelli A, Bucci C, Alifano M, Alifano P. Molecular docking
826 simulation reveals ACE2 polymorphisms that may increase the affinity of ACE2 with the SARS-
827 CoV-2 Spike protein. Biochimie. 2021;180:143-8.
828 46. Khayat AS, de Assumpcao PP, Meireles Khayat BC, Thomaz Araujo TM, Batista-
829 Gomes JA, Imbiriba LC, et al. ACE2 polymorphisms as potential players in COVID-19
830 outcome. PLoS One. 2020;15(12):e0243887.
831 47. Busnadiego I, Fernbach S, Pohl MO, Karakus U, Huber M, Trkola A, et al. Antiviral
832 Activity of Type I, II, and III Interferons Counterbalances ACE2 Inducibility and Restricts
833 SARS-CoV-2. mBio. 2020;11(5).
834 48. Cheemarla NR, Watkins TA, Mihaylova VT, Wang B, Zhao D, Wang G, et al.
835 Magnitude and timing of the antiviral response determine SARS-CoV-2 replication early in
836 infection. medRxiv. 2021.
837 49. Lowery SA, Sariol A, Perlman S. Innate immune and inflammatory responses to SARS-
838 CoV-2: Implications for COVID-19. Cell Host Microbe. 2021.

839 50. Sato T, Stange DE, Ferrante M, Vries RG, Van Es JH, Van den Brink S, et al. Long-term
840 expansion of epithelial organoids from human colon, adenoma, adenocarcinoma, and Barrett's
841 epithelium. Gastroenterology. 2011;141(5):1762-72.
842 51. Middendorp S, Schneeberger K, Wiegerinck CL, Mokry M, Akkerman RD, van
843 Wijngaarden S, et al. Adult stem cells in the small intestine are intrinsically programmed with
844 their location-specific function. Stem Cells. 2014;32(5):1083-91.
845 52. Lei X, Dong X, Ma R, Wang W, Xiao X, Tian Z, et al. Activation and evasion of type I
846 interferon responses by SARS-CoV-2. Nat Commun. 2020;11(1):3810.
847 53. Chen X, Saccon E, Appelberg KS, Mikaeloff F, Rodriguez JE, Vinhas BS, et al. Type-I
848 interferon signatures in SARS-CoV-2 infected Huh7 cells. Cell Death Discov. 2021;7(1):114.
849 54. Ghoshal K, Majumder S, Zhu Q, Hunzeker J, Datta J, Shah M, et al. Influenza virus
850 infection induces metallothionein gene expression in the mouse liver and lung by overlapping
851 but distinct molecular mechanisms. Mol Cell Biol. 2001;21(24):8301-17.
852 55. Ilback NG, Glynn AW, Wikberg L, Netzel E, Lindh U. Metallothionein is induced and
853 trace element balance changed in target organs of a common viral infection. Toxicology.
854 2004;199(2-3):241-50.
855 56. Pedersen KB, Chodavarapu H, Lazartigues E. Forkhead Box Transcription Factors of the
856 FOXA Class Are Required for Basal Transcription of Angiotensin-Converting Enzyme 2. J
857 Endocr Soc. 2017;1(4):370-84.
858 57. Yang J, Feng X, Zhou Q, Cheng W, Shang C, Han P, et al. Pathological Ace2-to-Ace
859 enzyme switch in the stressed heart is transcriptionally controlled by the endothelial Brg1-
860 FoxM1 complex. Proc Natl Acad Sci U S A. 2016;113(38):E5628-35.
861 58. Tada T, Fan C, Chen JS, Kaur R, Stapleford KA, Gristick H, et al. An ACE2 Microbody
862 Containing a Single Immunoglobulin Fc Domain Is a Potent Inhibitor of SARS-CoV-2. Cell
863 Rep. 2020;33(12):108528.
864 59. Wu L, Zhou L, Mo M, Liu T, Wu C, Gong C, et al. SARS-CoV-2 Omicron RBD shows
865 weaker binding affinity than the currently dominant Delta variant to human ACE2. Signal
866 Transduct Target Ther. 2022;7(1):8.
867 60. Mannar D, Saville JW, Zhu X, Srivastava SS, Berezuk AM, Tuttle KS, et al. SARS-
868 CoV-2 Omicron Variant: ACE2 Binding, Cryo-EM Structure of Spike Protein-ACE2 Complex
869 and Antibody Evasion. bioRxiv. 2021:2021.12.19.473380.
870 61. Peacock TP, Brown JC, Zhou J, Thakur N, Newman J, Kugathasan R, et al. The SARS-
871 CoV-2 variant, Omicron, shows rapid replication in human primary nasal epithelial cultures and
872 efficiently uses the endosomal route of entry. bioRxiv. 2022:2021.12.31.474653.
873 62. Carrera G, Paternain JL, Carrere N, Folch J, Courtade-Saidi M, Orfila C, et al. Hepatic
874 metallothionein in patients with chronic hepatitis C: relationship with severity of liver disease
875 and response to treatment. Am J Gastroenterol. 2003;98(5):1142-9.
876 63. Read SA, Parnell G, Booth D, Douglas MW, George J, Ahlenstiel G. The antiviral role
877 of zinc and metallothioneins in hepatitis C infection. J Viral Hepat. 2018;25(5):491-501.
878 64. Panchariya L, Khan WA, Kuila S, Sonkar K, Sahoo S, Ghoshal A, et al. Zinc(2+) ion
879 inhibits SARS-CoV-2 main protease and viral replication in vitro. Chem Commun (Camb).
880 2021;57(78):10083-6.
881 65. Kanekiyo M, Itoh N, Kawasaki A, Tanaka J, Nakanishi T, Tanaka K. Zinc-induced
882 activation of the human cytomegalovirus major immediate-early promoter is mediated by
883 metallothionein and nuclear factor-kappaB. Toxicol Appl Pharmacol. 2001;173(3):146-53.

884 66. Abt MC, Buffie CG, Susac B, Becattini S, Carter RA, Leiner I, et al. TLR-7 activation
885 enhances IL-22-mediated colonization resistance against vancomycin-resistant enterococcus. Sci
886 Transl Med. 2016;8(327):327ra25.
887 67. Kernbauer E, Ding Y, Cadwell K. An enteric virus can replace the beneficial function of
888 commensal bacteria. Nature. 2014;516(7529):94-8.
889 68. Neil JA, Matsuzawa-Ishimoto Y, Kernbauer-Holzl E, Schuster SL, Sota S, Venzon M, et
890 al. IFN-I and IL-22 mediate protective effects of intestinal viral infection. Nat Microbiol.
891 2019;4(10):1737-49.
892 69. Van Winkle JA, Constant DA, Li L, Nice TJ. Selective Interferon Responses of
893 Intestinal Epithelial Cells Minimize Tumor Necrosis Factor Alpha Cytotoxicity. J Virol.
894 2020;94(21).
895 70. Sun L, Miyoshi H, Origanti S, Nice TJ, Barger AC, Manieri NA, et al. Type I
896 Interferons Link Viral Infection to Enhanced Epithelial Turnover and Repair. Cell Host Microbe.
897 2014.
898 71. Aden K, Tran F, Ito G, Sheibani-Tezerji R, Lipinski S, Kuiper JW, et al. ATG16L1
899 orchestrates interleukin-22 signaling in the intestinal epithelium via cGAS-STING. J Exp Med.
900 2018;215(11):2868-86.
901 72. Liu L, Gong T, Tao W, Lin B, Li C, Zheng X, et al. Commensal viruses maintain
902 intestinal intraepithelial lymphocytes via noncanonical RIG-I signaling. Nat Immunol.
903 2019;20(12):1681-91.
904 73. Broggi A, Tan Y, Granucci F, Zanoni I. IFN-lambda suppresses intestinal inflammation
905 by non-translational regulation of neutrophil function. Nat Immunol. 2017;18(10):1084-93.
906 74. Yang JY, Kim MS, Kim E, Cheon JH, Lee YS, Kim Y, et al. Enteric Viruses Ameliorate
907 Gut Inflammation via Toll-like Receptor 3 and Toll-like Receptor 7-Mediated Interferon-beta
908 Production. Immunity. 2016;44(4):889-900.
909 75. Martin PK, Marchiando A, Xu R, Rudensky E, Yeung F, Schuster SL, et al. Autophagy
910 proteins suppress protective type I interferon signalling in response to the murine gut microbiota.
911 Nat Microbiol. 2018;3(10):1131-41.
912 76. Matsuzawa-Ishimoto Y, Shono Y, Gomez LE, Hubbard-Lucey VM, Cammer M, Neil J,
913 et al. Autophagy protein ATG16L1 prevents necroptosis in the intestinal epithelium. J Exp Med.
914 2017;214(12):3687-705.
915 77. Wu Y, Cheng X, Jiang G, Tang H, Ming S, Tang L, et al. Altered oral and gut
916 microbiota and its association with SARS-CoV-2 viral load in COVID-19 patients during
917 hospitalization. NPJ Biofilms Microbiomes. 2021;7(1):61.
918 78. Yeoh YK, Zuo T, Lui GC, Zhang F, Liu Q, Li AY, et al. Gut microbiota composition
919 reflects disease severity and dysfunctional immune responses in patients with COVID-19. Gut.
920 2021;70(4):698-706.
921 79. Zhang F, Wan Y, Zuo T, Yeoh YK, Liu Q, Zhang L, et al. Prolonged Impairment of
922 Short-Chain Fatty Acid and L-Isoleucine Biosynthesis in Gut Microbiome in Patients With
923 COVID-19. Gastroenterology. 2021.
924 80. Venzon M, Bernard L, Klein J, Axelrad JE, Hussey GA, Sullivan AP, et al. Gut
925 microbiome dysbiosis during COVID-19 is associated with increased risk for bacteremia and
926 microbial translocation. bioRxiv. 2021:2021.07.15.452246.
927 81. Vandesompele J, De Preter K, Pattyn F, Poppe B, Van Roy N, De Paepe A, et al.
928 Accurate normalization of real-time quantitative RT-PCR data by geometric averaging of
929 multiple internal control genes. Genome Biol. 2002;3(7):RESEARCH0034.

930 82. Li W, Moore MJ, Vasilieva N, Sui J, Wong SK, Berne MA, et al. Angiotensin-
931 converting enzyme 2 is a functional receptor for the SARS coronavirus. Nature.
932 2003;426(6965):450-4.
933 83. Xie X, Muruato A, Lokugamage KG, Narayanan K, Zhang X, Zou J, et al. An Infectious
934 cDNA Clone of SARS-CoV-2. Cell Host Microbe. 2020;27(5):841-8 e3.
935 84. Lee IT, Nakayama T, Wu CT, Goltsev Y, Jiang S, Gall PA, et al. ACE2 localizes to the
936 respiratory cilia and is not increased by ACE inhibitors or ARBs. Nat Commun.
937 2020;11(1):5453.
938 85. Tada T, Zhou H, Dcosta BM, Samanovic MI, Chivukula V, Herati RS, et al. Increased
939 resistance of SARS-CoV-2 Omicron Variant to Neutralization by Vaccine-Elicited and
940 Therapeutic Antibodies. bioRxiv. 2021:2021.12.28.474369.
941

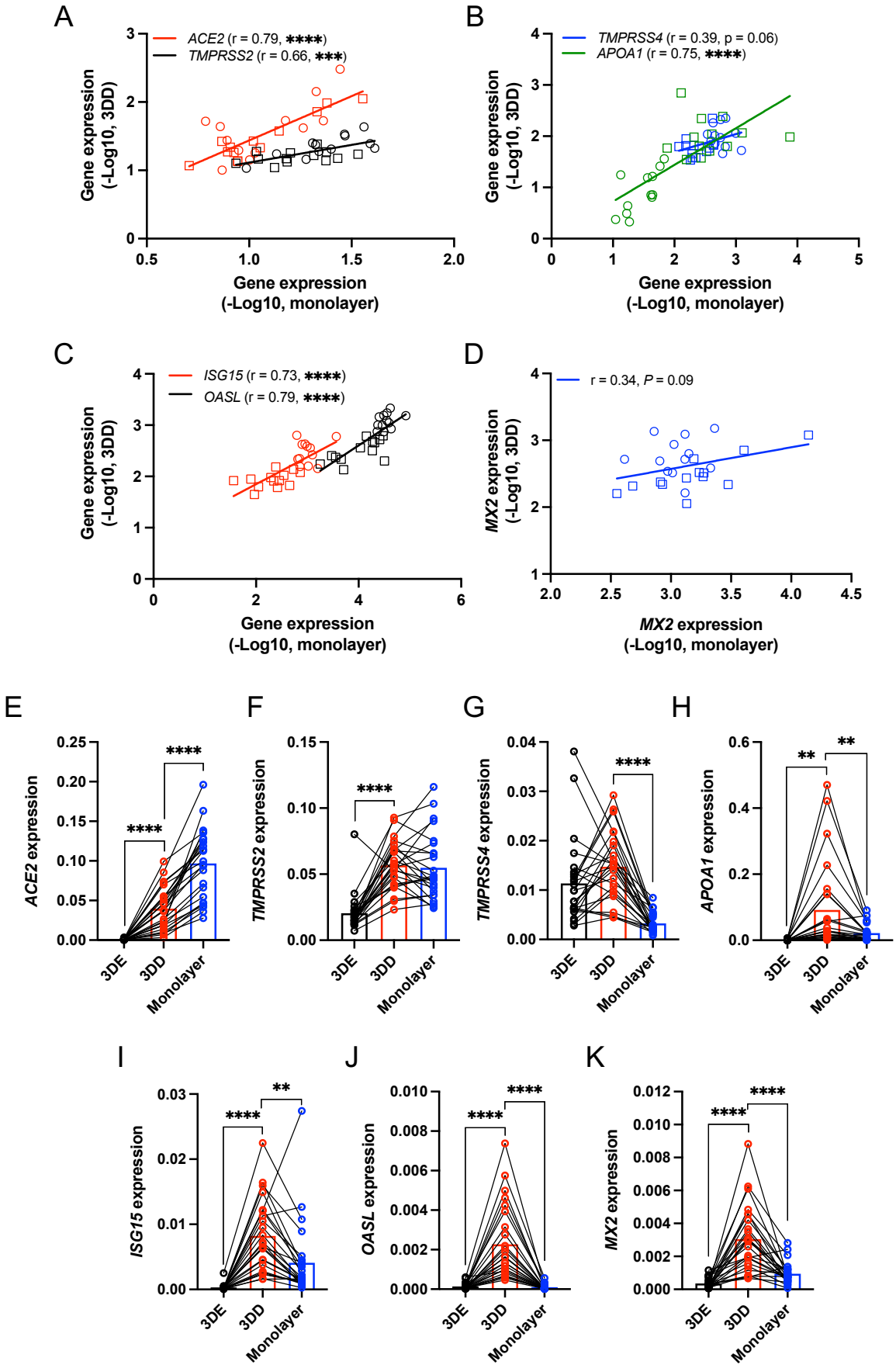
A
ACE2 (r = 0.79, ****)
TMPRSS2 (r = 0.66, ***)
Gene expression (-Log10, 3DD)
Gene expression (-Log10, monolayer)
B
TMPRSS4 (r = 0.39, p = 0.06)
APOA1 (r = 0.75, ****)
Gene expression (-Log10, 3DD)
Gene expression (-Log10, monolayer)
C
ISG15 (r = 0.73, ****)
OASL (r = 0.79, ****)
Gene expression (-Log10, 3DD)
Gene expression (-Log10, monolayer)
D
r = 0.34, P = 0.09
MX2 expression (-Log10, 3DD)
MX2 expression (-Log10, monolayer)
E
ACE2 expression
F
TMPRSS2 expression
G
TMPRSS4 expression
H
APOA1 expression
I
ISG15 expression
J
OASL expression
K
MX2 expression
3DE
3DD
Monolayer

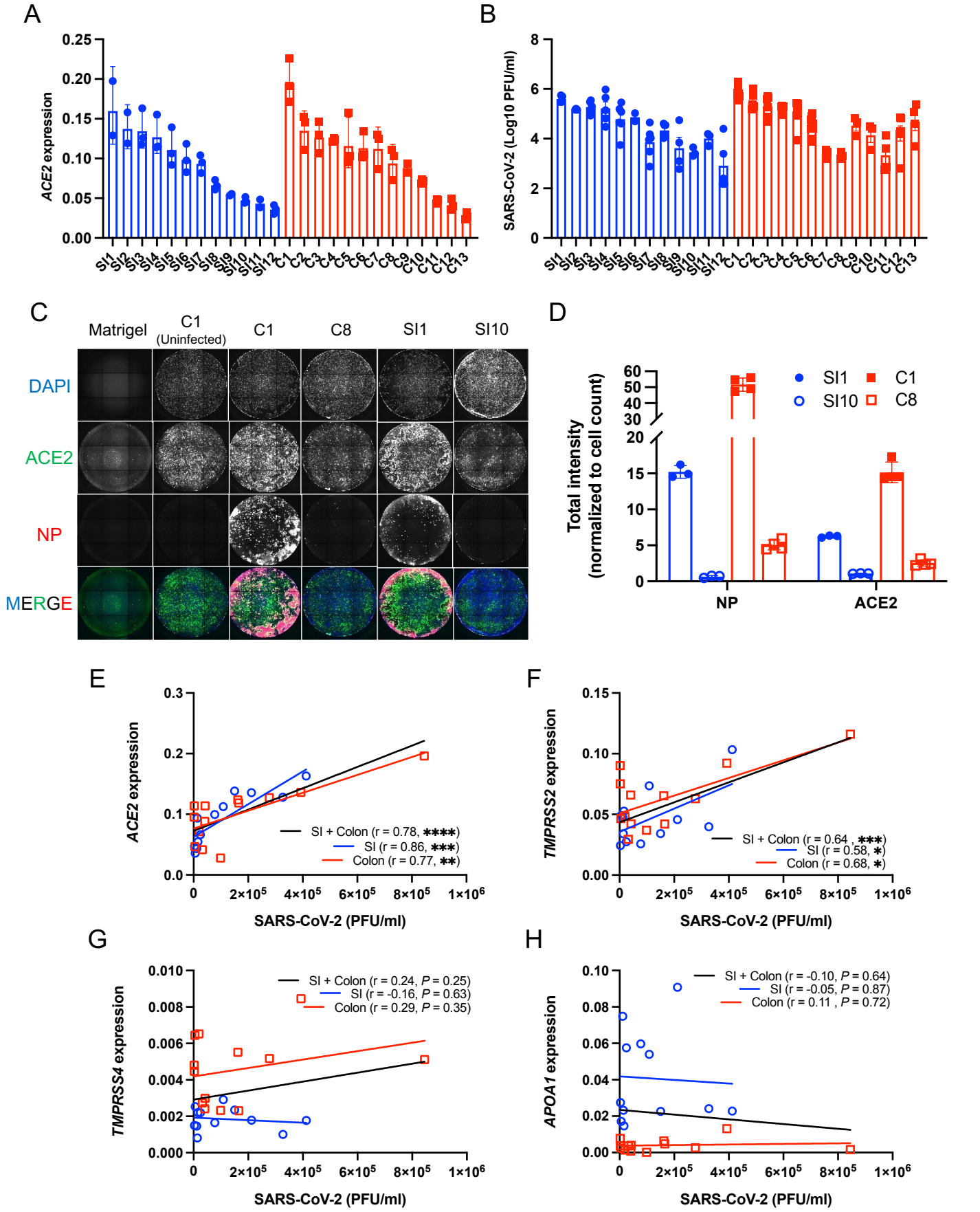
A
ACE2 expression
0.25
0.20
0.15
0.10
0.05
0.00
SI1 SI2 SI3 SI4 SI5 SI6 SI7 SI8 SI9 SI10 SI11 SI12 C1 C2 C3 C4 C5 C6 C7 C8 C9 C10 C11 C12 C13
B
SARS-CoV-2 (Log10 PFU/ml)
8
6
4
2
0
SI1 SI2 SI3 SI4 SI5 SI6 SI7 SI8 SI9 SI10 SI11 SI12 C1 C2 C3 C4 C5 C6 C7 C8 C9 C10 C11 C12 C13
C
Matrigel
C1 (Uninfected)
C1
C8
SI1
SI10
DAPI
ACE2
NP
MERGE
D
Total intensity (normalized to cell count)
60
50
40
30
20
15
10
5
0
SI1
SI10
C1
C8
NP
ACE2
E
ACE2 expression
0.3
0.2
0.1
0.0
SI + Colon (r = 0.78, ****)
SI (r = 0.86, ***)
Colon (r = 0.77, **)
0
2×10^5
4×10^5
6×10^5
8×10^5
1×10^6
SARS-CoV-2 (PFU/ml)
F
TMPRSS2 expression
0.15
0.10
0.05
0.00
SI + Colon (r = 0.64 , ***)
SI (r = 0.58, *)
Colon (r = 0.68, *)
0
2×10^5
4×10^5
6×10^5
8×10^5
1×10^6
SARS-CoV-2 (PFU/ml)
G
TMPRSS4 expression
0.010
0.008
0.006
0.004
0.002
0.000
SI + Colon (r = 0.24, P = 0.25)
SI (r = -0.16, P = 0.63)
Colon (r = 0.29, P = 0.35)
0
2×10^5
4×10^5
6×10^5
8×10^5
1×10^6
SARS-CoV-2 (PFU/ml)
H
APOA1 expression
0.10
0.08
0.06
0.04
0.02
0.00
SI + Colon (r = -0.10, P = 0.64)
SI (r = -0.05, P = 0.87)
Colon (r = 0.11 , P = 0.72)
0
2×10^5
4×10^5
6×10^5
8×10^5
1×10^6
SARS-CoV-2 (PFU/ml)

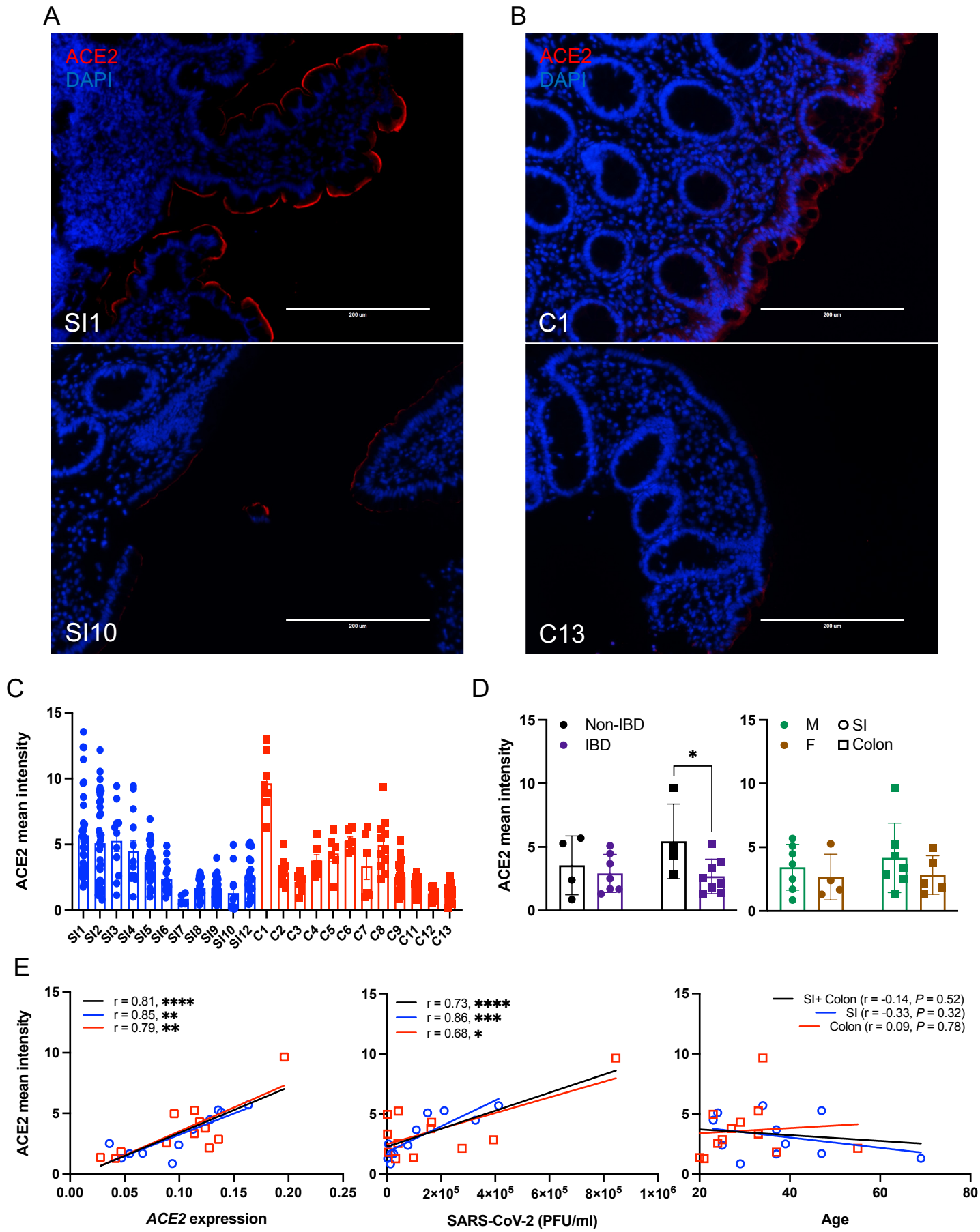
A
ACE2
DAPI
SI1
SI10
B
ACE2
DAPI
C1
C13
C
ACE2 mean intensity
SI1 SI2 SI3 SI4 SI5 SI6 SI7 SI8 SI9 SI10 SI12 C1 C2 C3 C4 C5 C6 C7 C8 C9 C11 C12 C13
D
ACE2 mean intensity
Non-IBD
IBD
*
M
F
SI
Colon
E
ACE2 mean intensity
r = 0.81, ****
r = 0.85, **
r = 0.79, **
ACE2 expression
r = 0.73, ****
r = 0.86, ***
r = 0.68, *
SARS-CoV-2 (PFU/ml)
SI+ Colon (r = -0.14, P = 0.52)
SI (r = -0.33, P = 0.32)
Colon (r = 0.09, P = 0.78)
Age

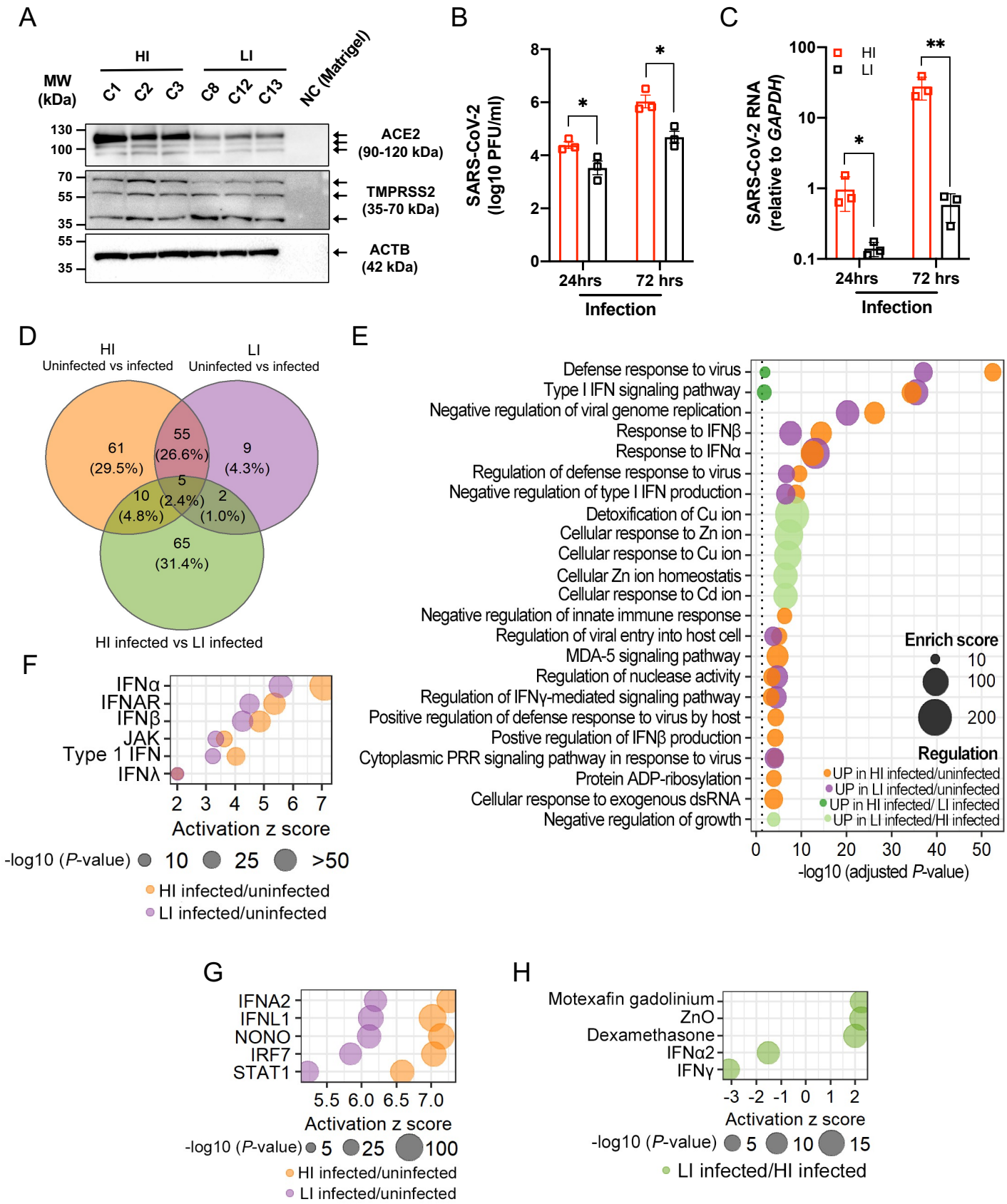
A
HI
LI
MW (kDa)
C1
C2
C3
C8
C12
C13
NC (Matrigel)
130
100
70
55
35
55
35
ACE2 (90-120 kDa)
TMPRSS2 (35-70 kDa)
ACTB (42 kDa)
B
SARS-CoV-2 (log10 PFU/ml)
24hrs
72 hrs
Infection
C
SARS-CoV-2 RNA (relative to GAPDH)
HI
LI
24hrs
72 hrs
Infection
D
HI Uninfected vs infected
LI Uninfected vs infected
61 (29.5%)
55 (26.6%)
9 (4.3%)
5 (2.4%)
10 (4.8%)
2 (1.0%)
65 (31.4%)
HI infected vs LI infected
E
Defense response to virus
Type I IFN signaling pathway
Negative regulation of viral genome replication
Response to IFNβ
Response to IFNα
Regulation of defense response to virus
Negative regulation of type I IFN production
Detoxification of Cu ion
Cellular response to Zn ion
Cellular response to Cu ion
Cellular Zn ion homeostatis
Cellular response to Cd ion
Negative regulation of innate immune response
Regulation of viral entry into host cell
MDA-5 signaling pathway
Regulation of nuclease activity
Regulation of IFNγ-mediated signaling pathway
Positive regulation of defense response to virus by host
Postive regulation of IFNβ production
Cytoplasmic PRR signaling pathway in response to virus
Protein ADP-ribosylation
Cellular response to exogenous dsRNA
Negative regulation of growth
Enrich score
10
100
200
Regulation
UP in HI infected/uninfected
UP in LI infected/uninfected
UP in HI infected/ LI infected
UP in LI infected/HI infected
-log10 (adjusted P-value)
F
IFNα
IFNAR
IFNβ
JAK
Type 1 IFN
IFNλ
Activation z score
-log10 (P-value) 10 25 >50
HI infected/uninfected
LI infected/uninfected
G
IFNA2
IFNL1
NONO
IRF7
STAT1
Activation z score
-log10 (P-value) 5 25 100
HI infected/uninfected
LI infected/uninfected
H
Motexafin gadolinium
ZnO
Dexamethasone
IFNα2
IFNγ
Activation z score
-log10 (P-value) 5 10 15
LI infected/HI infected

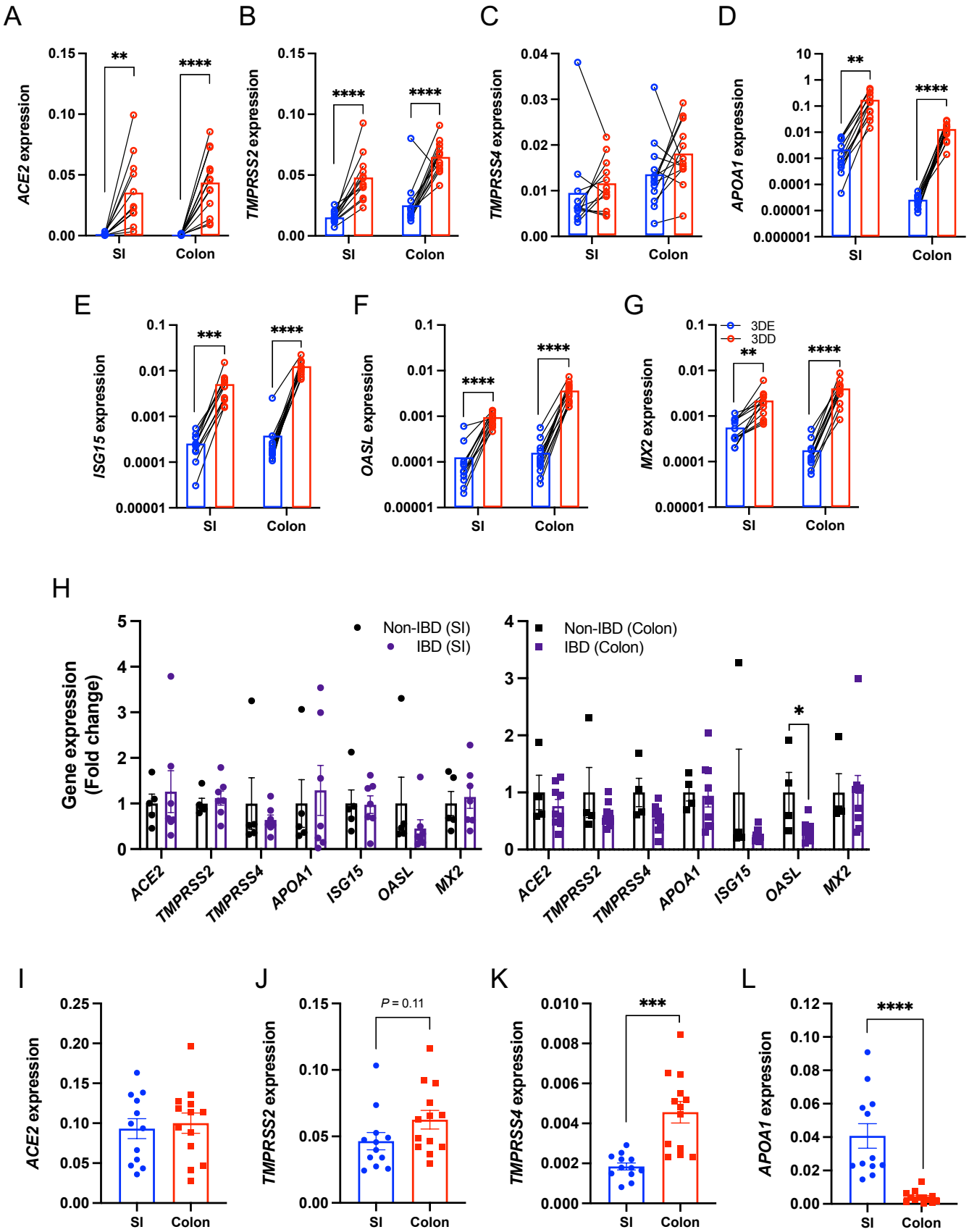
A
ACE2 expression
0.15
0.10
0.05
0.00
**
****
SI
Colon
B
TMPRSS2 expression
0.15
0.10
0.05
0.00
****
****
SI
Colon
C
TMPRSS4 expression
0.04
0.03
0.02
0.01
0.00
SI
Colon
D
APOA1 expression
10
1
0.1
0.01
0.001
0.0001
0.00001
0.000001
**
****
SI
Colon
E
ISG15 expression
0.1
0.01
0.001
0.0001
0.00001
***
****
SI
Colon
F
OASL expression
0.1
0.01
0.001
0.0001
0.00001
****
****
SI
Colon
G
MX2 expression
0.1
0.01
0.001
0.0001
0.00001
3DE
3DD
**
****
SI
Colon
H
Gene expression
(Fold change)
Non-IBD (SI)
IBD (SI)
Non-IBD (Colon)
IBD (Colon)
*
ACE2
TMPRSS2
TMPRSS4
APOA1
ISG15
OASL
MX2
I
ACE2 expression
0.25
0.20
0.15
0.10
0.05
0.00
SI
Colon
J
TMPRSS2 expression
0.15
0.10
0.05
0.00
P = 0.11
SI
Colon
K
TMPRSS4 expression
0.010
0.008
0.006
0.004
0.002
0.000
***
SI
Colon
L
APOA1 expression
0.12
0.10
0.08
0.06
0.04
0.02
0.00
****
SI
Colon

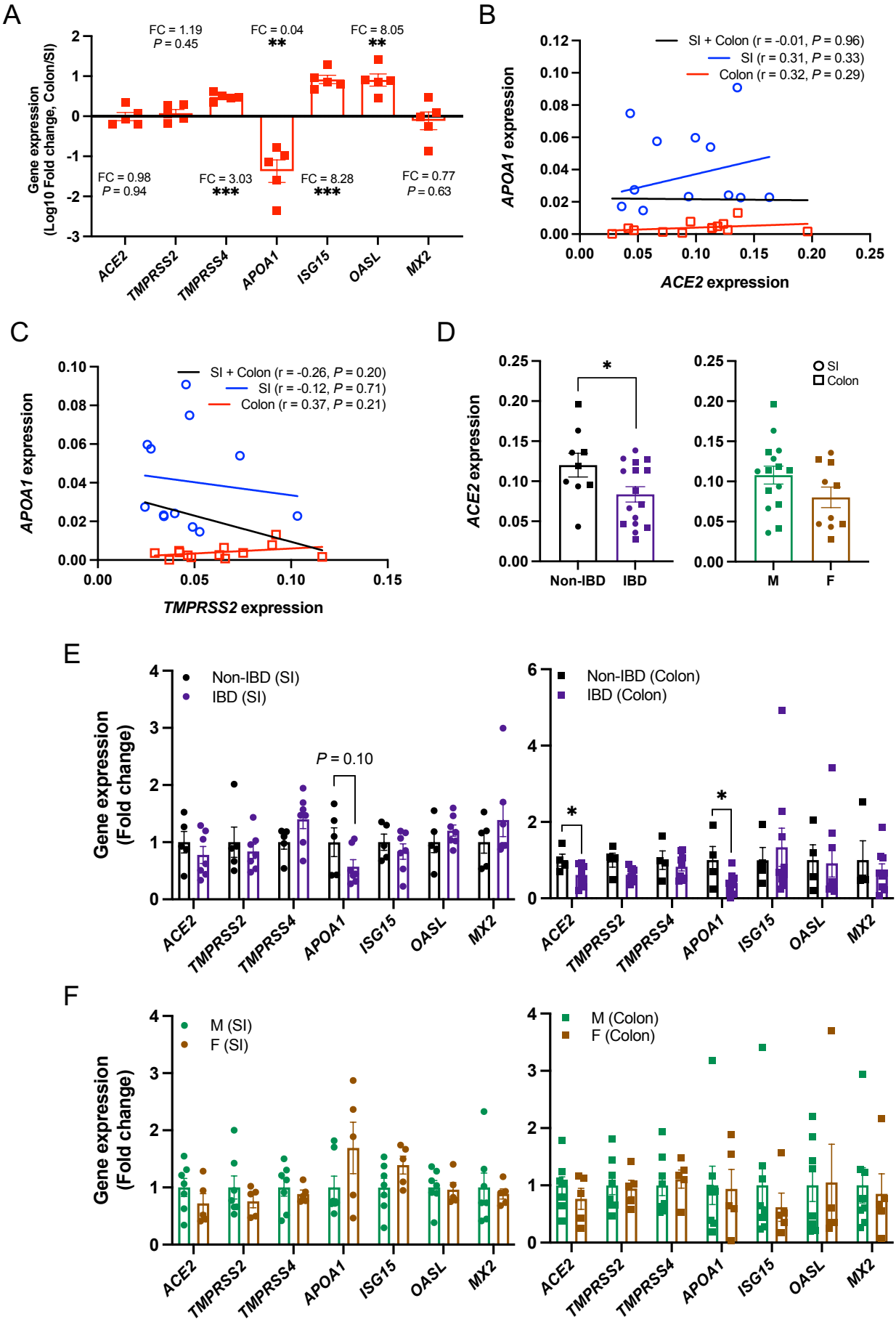
A
Gene expression (Log10 Fold change, Colon/SI)
FC = 1.19 P = 0.45
FC = 0.04 **
FC = 8.05 **
FC = 0.98 P = 0.94
FC = 3.03 ***
FC = 8.28 ***
FC = 0.77 P = 0.63
ACE2
TMPRSS2
TMPRSS4
APOA1
ISG15
OASL
MX2
B
SI + Colon (r = -0.01, P = 0.96)
SI (r = 0.31, P = 0.33)
Colon (r = 0.32, P = 0.29)
APOA1 expression
ACE2 expression
C
SI + Colon (r = -0.26, P = 0.20)
SI (r = -0.12, P = 0.71)
Colon (r = 0.37, P = 0.21)
APOA1 expression
TMPRSS2 expression
D
ACE2 expression
Non-IBD
IBD
SI
Colon
M
F
E
Non-IBD (SI)
IBD (SI)
P = 0.10
Non-IBD (Colon)
IBD (Colon)
Gene expression (Fold change)
F
M (SI)
F (SI)
M (Colon)
F (Colon)

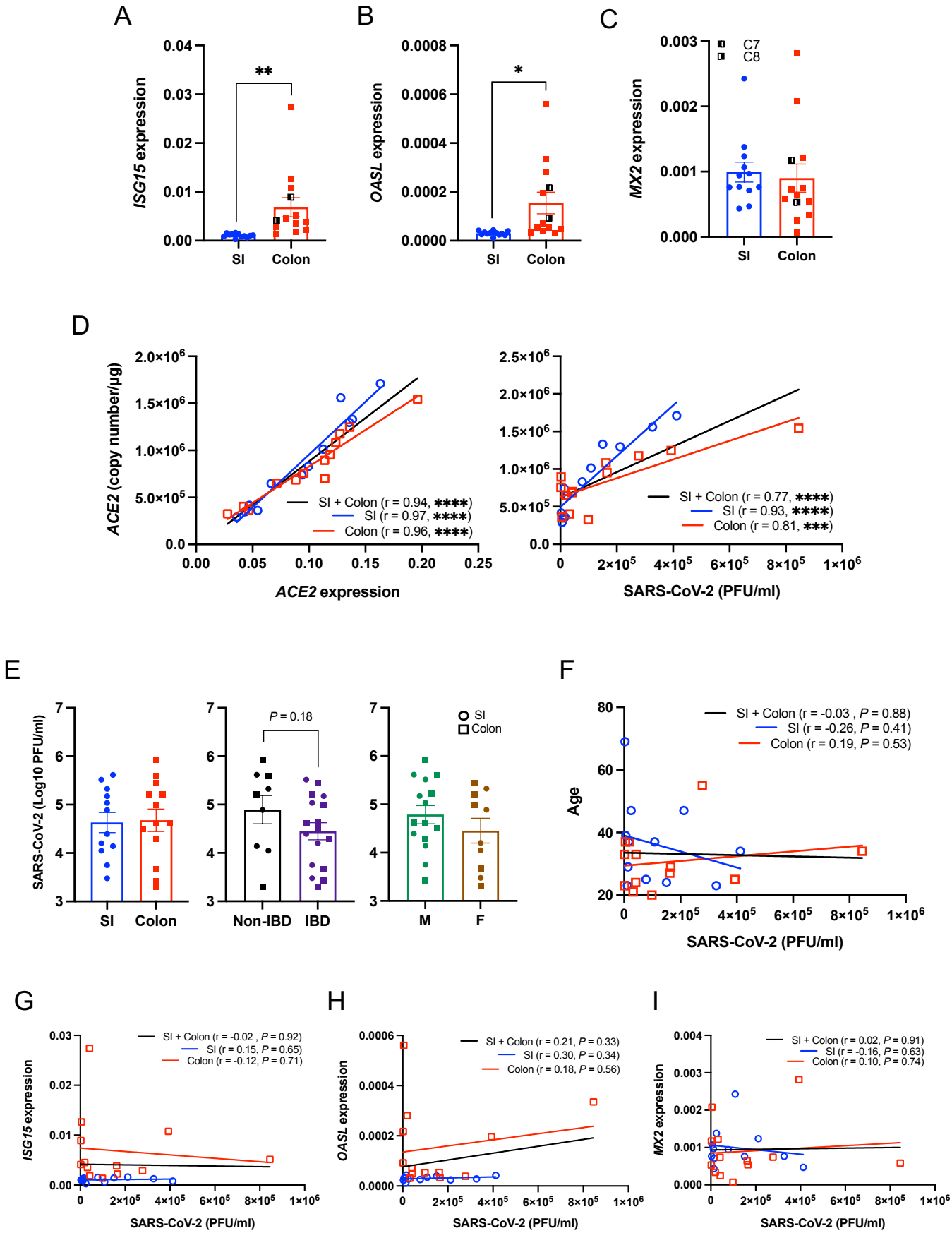
A
ISG15 expression
0.04
0.03
0.02
0.01
0.00
**
SI
Colon
B
OASL expression
0.0008
0.0006
0.0004
0.0002
0.0000
*
SI
Colon
C
MX2 expression
0.003
0.002
0.001
0.000
C7
C8
SI
Colon
D
ACE2 (copy number/μg)
2.0×10^6
1.5×10^6
1.0×10^6
5.0×10^5
0.0
0.00
0.05
0.10
0.15
0.20
0.25
ACE2 expression
SI + Colon (r = 0.94, ****)
SI (r = 0.97, ****)
Colon (r = 0.96, ****)
2.5×10^6
2.0×10^6
1.5×10^6
1.0×10^6
5.0×10^5
0.0
0
2×10^5
4×10^5
6×10^5
8×10^5
1×10^6
SARS-CoV-2 (PFU/ml)
SI + Colon (r = 0.77, ****)
SI (r = 0.93, ****)
Colon (r = 0.81, ***)
E
SARS-CoV-2 (Log10 PFU/ml)
7
6
5
4
3
SI
Colon
P = 0.18
Non-IBD
IBD
SI
Colon
M
F
F
Age
80
60
40
20
0
2×10^5
4×10^5
6×10^5
8×10^5
1×10^6
SARS-CoV-2 (PFU/ml)
SI + Colon (r = -0.03 , P = 0.88)
SI (r = -0.26, P = 0.41)
Colon (r = 0.19, P = 0.53)
G
ISG15 expression
0.03
0.02
0.01
0.00
SI + Colon (r = -0.02 , P = 0.92)
SI (r = 0.15, P = 0.65)
Colon (r = -0.12, P = 0.71)
0
2×10^5
4×10^5
6×10^5
8×10^5
1×10^6
SARS-CoV-2 (PFU/ml)
H
OASL expression
0.0006
0.0004
0.0002
0.0000
SI + Colon (r = 0.21, P = 0.33)
SI (r = 0.30, P = 0.34)
Colon (r = 0.18, P = 0.56)
0
2×10^5
4×10^5
6×10^5
8×10^5
1×10^6
SARS-CoV-2 (PFU/ml)
I
MX2 expression
0.004
0.003
0.002
0.001
0.000
SI + Colon (r = 0.02, P = 0.91)
SI (r = -0.16, P = 0.63)
Colon (r = 0.10, P = 0.74)
0
2×10^5
4×10^5
6×10^5
8×10^5
1×10^6
SARS-CoV-2 (PFU/ml)

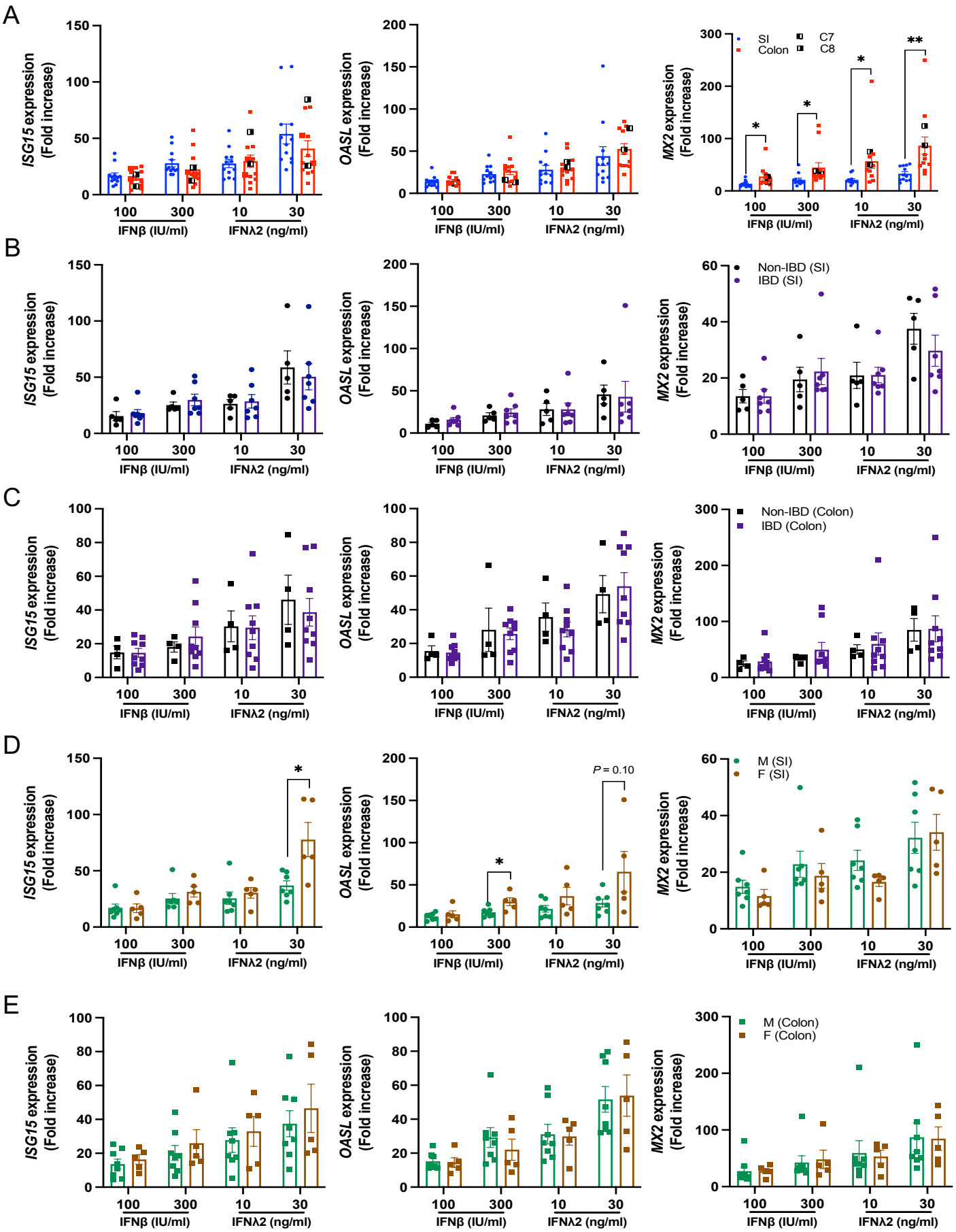
A
B
C
D
E
ISG15 expression (Fold increase)
OASL expression (Fold increase)
MX2 expression (Fold increase)
IFNβ (IU/ml)
IFNλ2 (ng/ml)
100
300
10
30
SI
Colon
C7
C8
Non-IBD (SI)
IBD (SI)
Non-IBD (Colon)
IBD (Colon)
M (SI)
F (SI)
M (Colon)
F (Colon)
P = 0.10

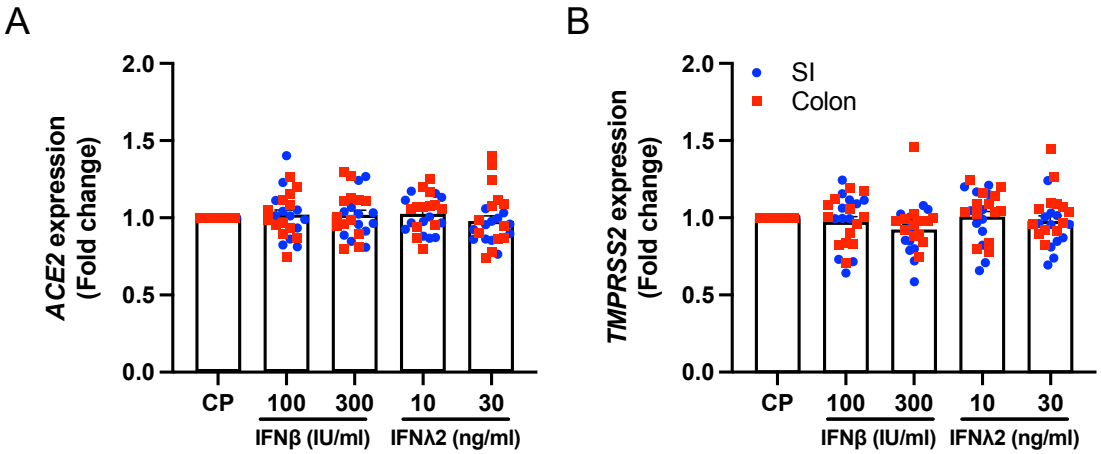
A
B
ACE2 expression
(Fold change)
TMPRSS2 expression
(Fold change)
2.0
1.5
1.0
0.5
0.0
SI
Colon
CP
100
300
10
30
IFNβ (IU/ml)
IFNλ2 (ng/ml)

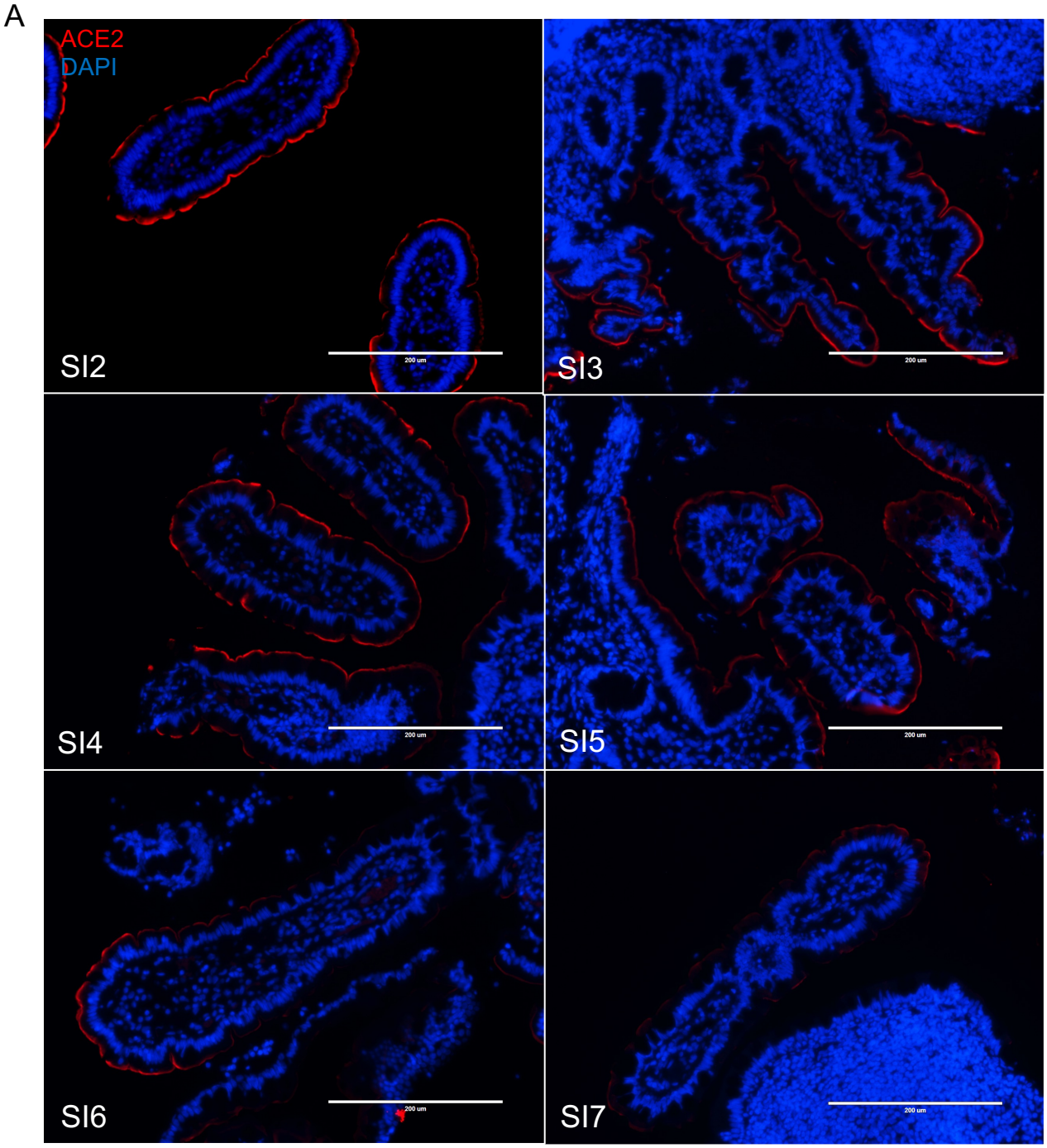
A
ACE2
DAPI
SI2
200 um
SI3
200 um
SI4
200 um
SI5
200 um
SI6
200 um
SI7
200 um

Supplemental Figure 6

A

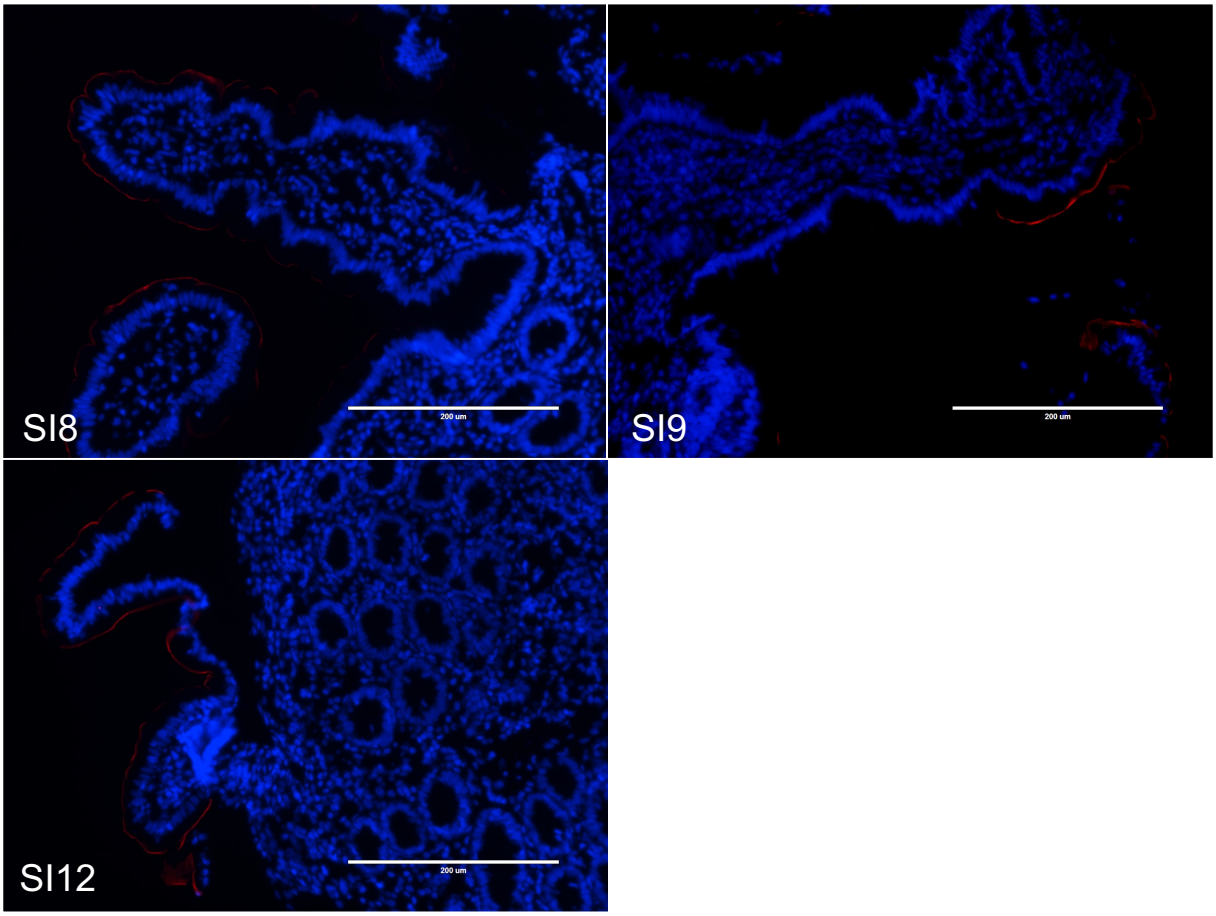

B

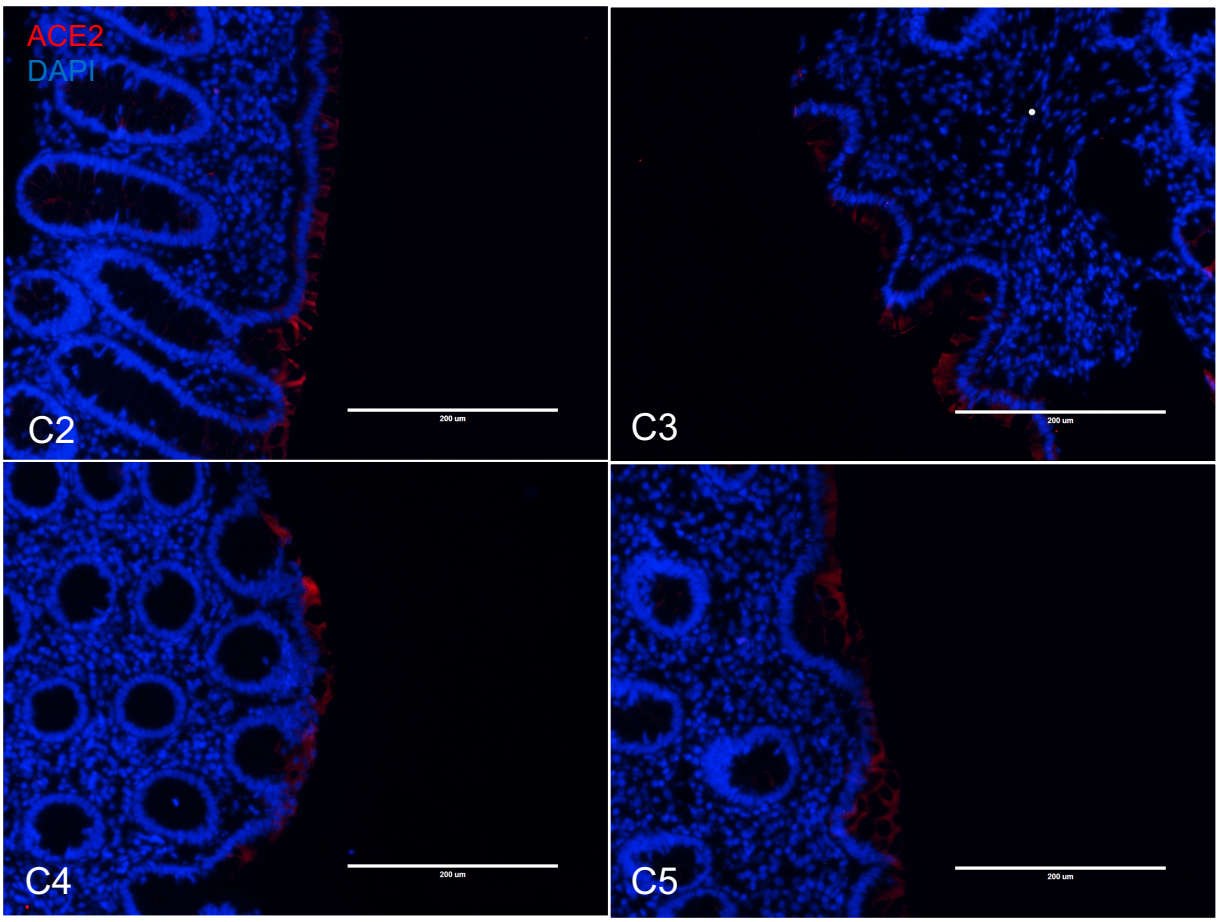

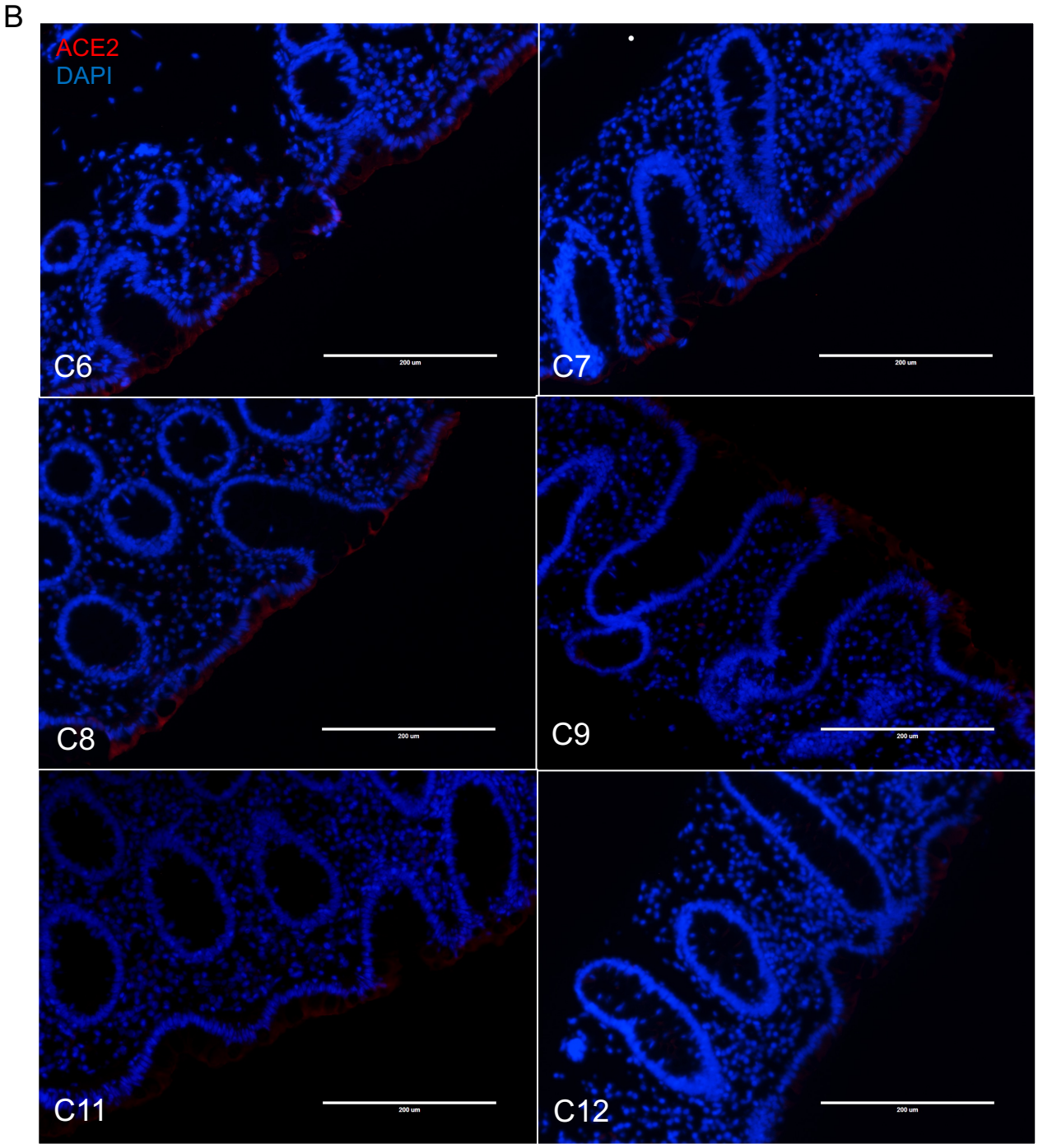
B
ACE2
DAPI
C6
200 um
C7
200 um
C8
200 um
C9
200 um
C11
200 um
C12
200 um

C

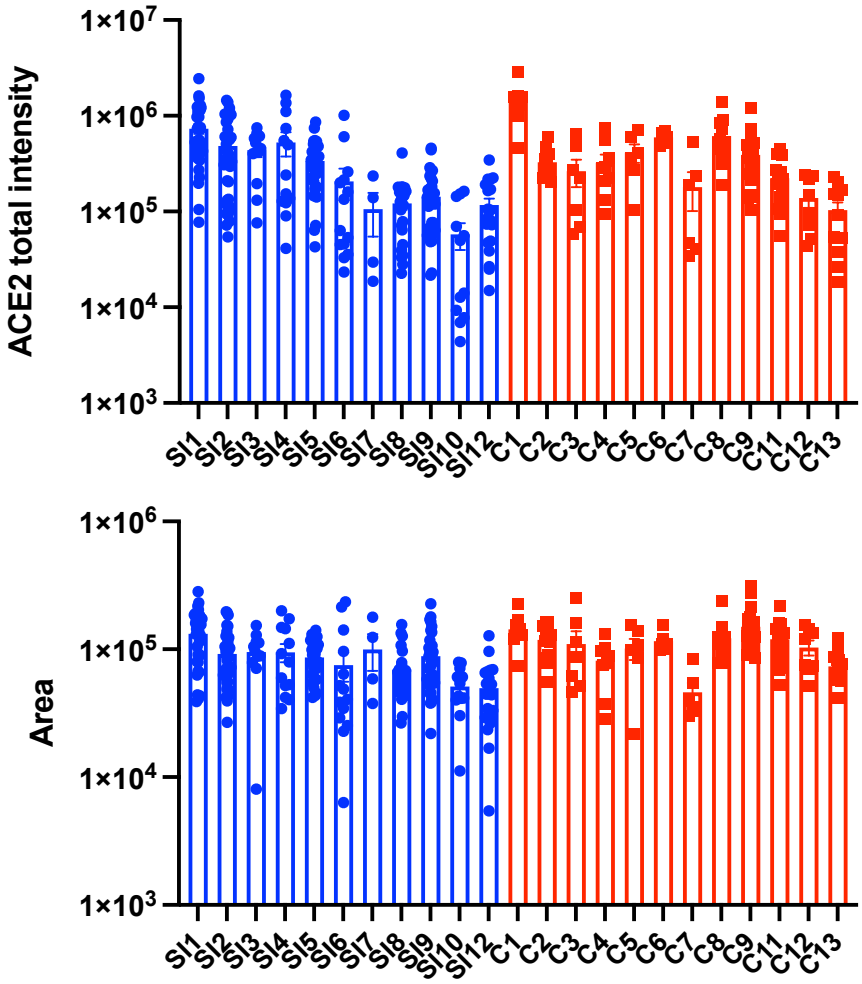
ACE2 total intensity
1×10^7
1×10^6
1×10^5
1×10^4
1×10^3
SI1 SI2 SI3 SI4 SI5 SI6 SI7 SI8 SI9 SI10 SI12 C1 C2 C3 C4 C5 C6 C7 C8 C9 C11 C12 C13
Area
1×10^6
1×10^5
1×10^4
1×10^3
SI1 SI2 SI3 SI4 SI5 SI6 SI7 SI8 SI9 SI10 SI12 C1 C2 C3 C4 C5 C6 C7 C8 C9 C11 C12 C13

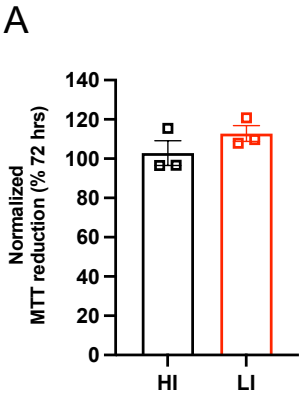

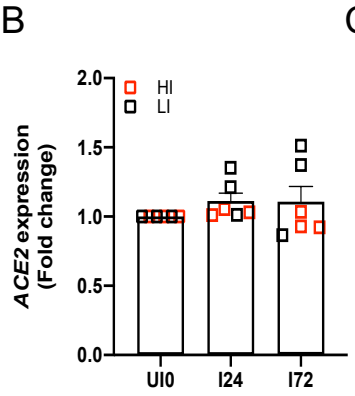

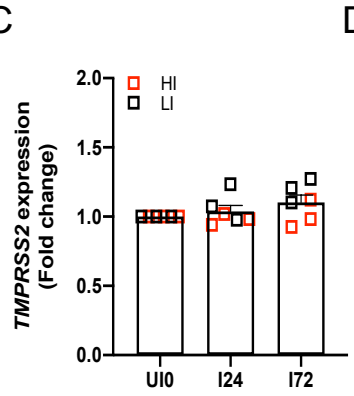

D

A vs B	Upregulated in	
	A	B
HI_UI0 vs LI_UI0	8	3
HI_UI72 vs LI_UI72	0	1
HI_I24 vs LI_I24	11	13
HI_I72 vs LI_I72	44	38
HI_UI0 vs HI_I24	10	3
HI_I24 vs HI_I72	12	180
HI_UI0 vs HI_UI72	0	0
HI_UI72 vs HI_I72	2	129
LI_UI0 vs LI_I24	7	0
LI_I24 vs LI_I72	46	207
LI_UI0 vs LI_UI72	0	0
LI_UI0 vs LI_I72	3	68

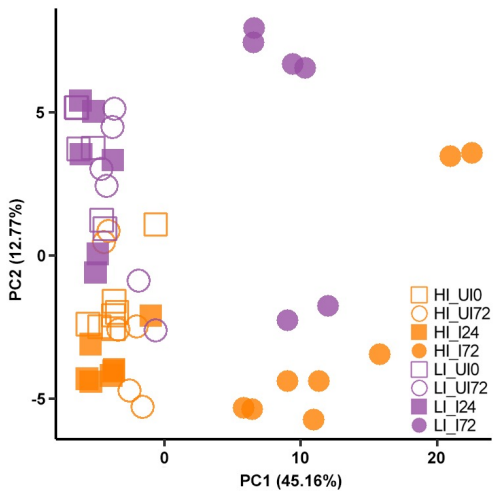

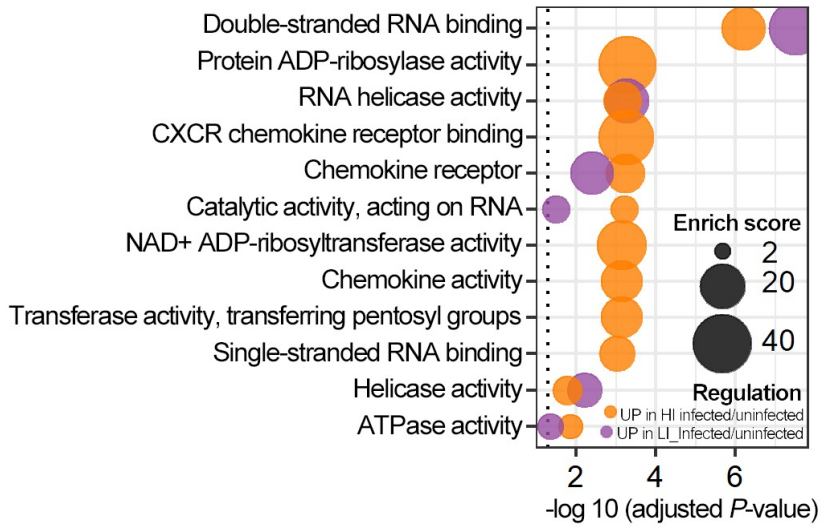

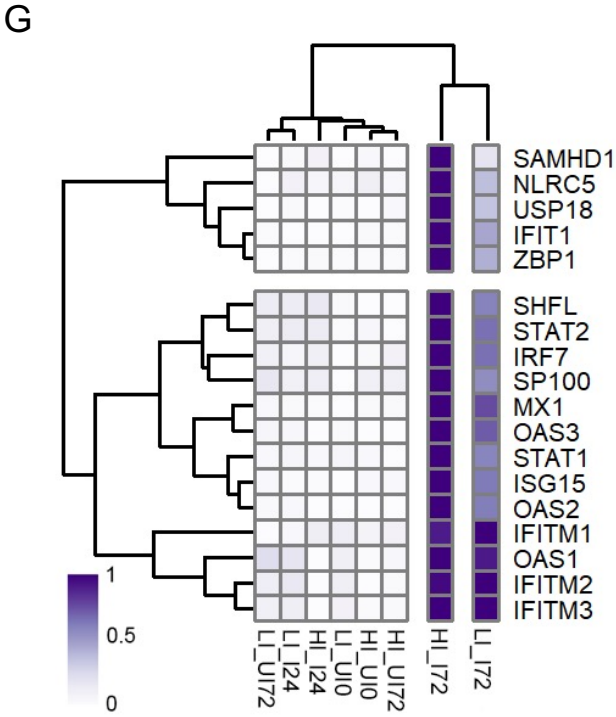

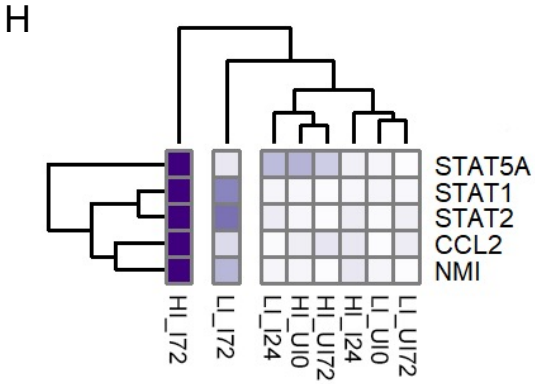

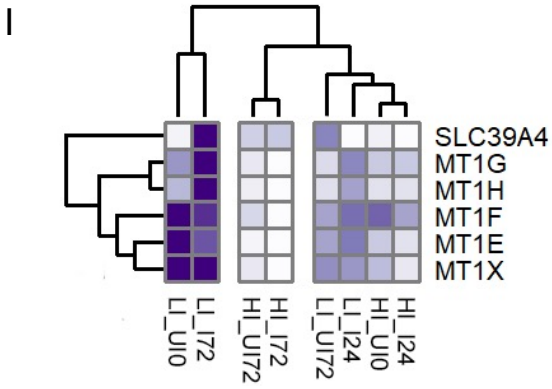

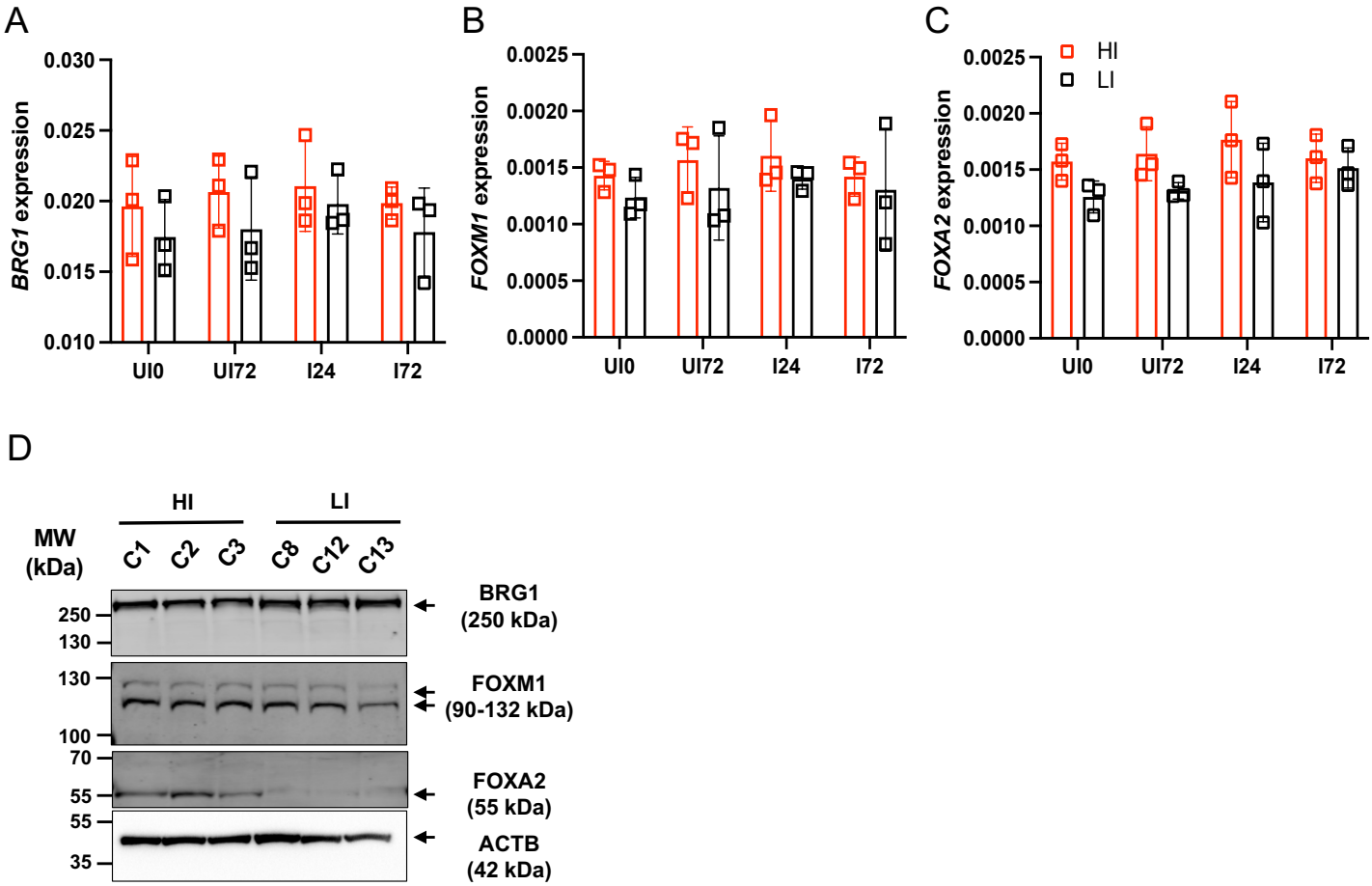
A
BRG1 expression
0.030
0.025
0.020
0.015
0.010
UI0
UI72
I24
I72
B
FOXM1 expression
0.0025
0.0020
0.0015
0.0010
0.0005
0.0000
UI0
UI72
I24
I72
C
FOXA2 expression
HI
LI
0.0025
0.0020
0.0015
0.0010
0.0005
0.0000
UI0
UI72
I24
I72
D
HI
LI
MW (kDa)
C1
C2
C3
C8
C12
C13
250
130
130
100
70
55
55
35
BRG1 (250 kDa)
FOXM1 (90-132 kDa)
FOXA2 (55 kDa)
ACTB (42 kDa)

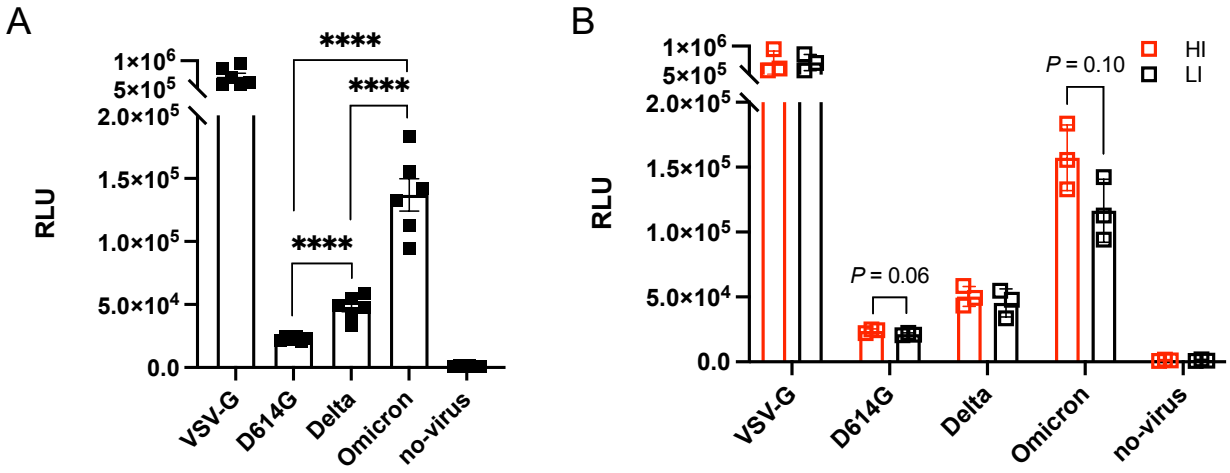
A
RLU
1×10^6
5×10^5
2.0×10^5
1.5×10^5
1.0×10^5
5.0×10^4
0.0
****
****
****
VSV-G
D614G
Delta
Omicron
no-virus
B
RLU
1×10^6
5×10^5
2.0×10^5
1.5×10^5
1.0×10^5
5.0×10^4
0.0
P = 0.06
P = 0.10
HI
LI
VSV-G
D614G
Delta
Omicron
no-virus